
Hydrodynamics of the cosmological quark-hadron transition in the presence of long-range energy and momentum transfer

John C. Miller^{1,2,3} & Luciano Rezzolla¹

¹Scuola Internazionale Superiore di Studi Avanzati, Trieste, Italy.

²Department of Physics, University of Oxford, England.

³Osservatorio Astronomico di Trieste, Trieste, Italy.

Abstract

Two previous papers in this series have presented a study of the growth of hadronic bubbles during the cosmological Quark–Hadron transition, treating the material within each phase as a single perfect fluid. Here, we extend the analysis to include the effects of long-range energy and momentum transfer by weakly and electromagnetically interacting particles. After a short review of the formalism adopted, we discuss the numerical strategies used in the computer code which has been constructed in order to solve this system of equations. Results for the growth of single hadronic bubbles are also presented.

PACS Nos.: 47.55.Dz, 47.75.+f, 95.30.Jx, 98.80.Cq

SISSA Ref. 161/94/A-EP (Oct 94)

I. Introduction

At about $10 \mu\text{s}$ after the big bang it is thought that strongly interacting matter underwent a transition from a plasma of free quarks and gluons to one in which the quarks were confined within hadrons (predominantly pions). Current lattice-gauge calculations [1] favour the view that this change may well have been a continuous one, but the possibility of it being a first order phase transition is by no means ruled out and considerable interest continues to be focussed on the astrophysical consequences which might have arisen if it was, indeed, first order (see, for example [2–4]).

The work described here (which is part of an ongoing research programme [5–8]) is within the scenario of a first-order transition starting with the nucleation of hadronic bubbles in a slightly supercooled quark-gluon plasma. The bubbles then proceed to grow (with the quark-gluon plasma being progressively transformed into a hadronic one) until eventually they coalesce and give rise to disconnected quark regions which then shrink and probably disappear completely (possibly leaving behind a significant baryon-number inhomogeneity) [9] but might instead reach a stable configuration composed of *strange quark matter* [10].

In the earlier papers of the series, attention has been focussed on studying the hydrodynamics of the growth of single hadronic bubbles during the initial stages of the transition where it makes sense to consider the material in each phase as a perfect fluid composed only of the strongly interacting matter. While the transition involves only these particles in a direct way, an important role is also played by other particles present, which can interact with them through the electromagnetic and weak interactions: primarily photons, electrons, muons and their antiparticles (electromagnetic and weak interactions) and neutrinos and antineutrinos (weak interaction only). All of these have mean free paths long compared with that of the strongly interacting matter and can provide a mechanism for long-range transport of energy and momentum through the strongly interacting fluid. Since the leptons concerned are essentially massless, both they and the photons can be treated as components of a generalized “radiation fluid” and the problem is then one of relativistic radiative transfer.

During bubble growth, the effect of this transport becomes significant when the radius R_s of the bubble surface becomes roughly comparable with the mean free path λ of the particles concerned ($\sim 10^4$ fermi for the electromagnetic interaction and ~ 1 cm for the weak interaction). When $R_s \ll \lambda$, the bubble is

essentially transparent to the radiation, which can then be ignored, while when $R_s \gg \lambda$ the coupling is essentially complete on relevant length-scales so that the radiation and strongly interacting matter move together as a single fluid. Clearly, the process of coupling can, in principle, occur twice during the bubble growth, but because the behaviour is similar in each case, we will discuss here only the one occurring between the strongly interacting and electromagnetically interacting particles. Identical considerations apply also for the coupling with the neutrinos, the only difference, apart from the scale, being the different number of degrees of freedom into which the energy liberated by the transition is channeled.

This paper is concerned with adding the effects of radiative transfer to our earlier scheme of calculation for following bubble growth [7], thus extending its range of validity. Subsequently, we aim to apply a similar scheme to the last stage of the transition (shrinking away of the disconnected quark regions) which is likely to give rise to the most interesting consequences from an astrophysical point of view. The formalism used for handling the radiative transfer has been the subject of an earlier paper [8] and only a brief outline of this will be presented again here.

The plan of the paper is as follows. In Section II we give a short review of the equations and then Section III describes the outline of our computational scheme which uses a combined characteristic and Lagrangian finite-difference approach. Some particular problems arise in the computational implementation and we explain how these have been overcome by means of introducing new variables for the radiation fluid. Section IV concerns the setting up of initial conditions, Section V describes tests carried out and results obtained and Section VI is the conclusion. Throughout, we use a system of units in which $c = \hbar = k_B = 1$ and a space-like signature $(-, +, +, +)$. Greek indices are taken to run from 0 to 3 and Latin indices from 1 to 3; covariant derivatives are denoted with a semi-colon and partial derivatives with a comma.

II. Relativistic Hydrodynamical Equations

This section contains a short review of the equations used in the rest of the paper. A full discussion of these has already been presented in [8] to which the reader is referred for further details and references.

The transfer of energy and momentum is considered as taking place between a *standard fluid*, composed of the strongly interacting particles and any other

particles effectively moving together with them, and a *radiation fluid* consisting of those particles responsible for the long-range transfer of energy and momentum. We treat the transfer using the PSTF (Projected Symmetric Trace Free) tensor formalism of Thorne [11], [12] in which the relativistic radiative transfer equation is rewritten in terms of an infinite hierarchy of differential equations involving PSTF moments which is then truncated by introducing suitable closure relations. For spherical symmetry, the tensor formalism becomes effectively a scalar one. We made the truncation at second order and obtained

$$(w_0)_{,t} + \frac{a}{b}(w_1)_{,\mu} + \frac{4}{3}\left(\frac{b_{,t}}{b} + \frac{2R_{,t}}{R}\right)w_0 + \frac{2a}{b}\left(\frac{a_{,\mu}}{a} + \frac{R_{,\mu}}{R}\right)w_1 + \left(\frac{b_{,t}}{b} - \frac{R_{,t}}{R}\right)w_2 = as_0, \quad (1)$$

$$(w_1)_{,t} + \frac{a}{b}\left(\frac{1}{3}w_0 + w_2\right)_{,\mu} + \frac{4a_{,\mu}}{3b}w_0 + 2\left(\frac{b_{,t}}{b} + \frac{R_{,t}}{R}\right)w_1 + \frac{a}{b}\left(\frac{a_{,\mu}}{a} + \frac{3R_{,\mu}}{R}\right)w_2 = as_1, \quad (2)$$

$$w_2 = f_E w_0, \quad (3)$$

where w_0 is the energy density of the radiation, w_1 is the radiation flux and w_2 is the anisotropy scalar of the radiation (all measured in the local rest frame of the standard fluid); s_0 and s_1 are energy and momentum source functions and a and b are metric coefficients of the spherically symmetric line element

$$ds^2 = -a^2 dt^2 + b^2 d\mu^2 + R^2(d\theta^2 + \sin^2\theta d\varphi^2), \quad (4)$$

where μ is a comoving radial coordinate and R is the associated Eulerean coordinate (the Schwarzschild circumference coordinate).

The quantity f_E appearing in the closure relation (3) is a *variable Eddington factor* which can take values ranging from 0, for complete isotropy (which could be caused by the medium being extremely optically thick), to 2/3 for complete anisotropy (which might arise when the medium is very optically thin). The expression used for it has to be arrived at on the basis of physical considerations and for our case we have used

$$f_E \equiv \frac{8u^2/9}{(1 + 4u^2/3)} \left(\frac{\lambda}{\lambda + R} \right), \quad (5)$$

where λ is the effective mean-free-path of the radiation particles. In our picture, the bubble is first nucleated within a uniform and isotropic quark medium and the radiation field (which interacts with the quark medium on suitably large scales and is in thermal equilibrium with it) initially shares these properties (*i.e.* w_0 is

constant everywhere and w_1 and w_2 are zero). The radius of the newly-formed bubble is small compared with λ and the medium is essentially transparent to the radiation on this scale. As the bubble starts to expand, the radiation quantities deviate from their values at the time of nucleation primarily as a result of the Doppler effect arising from the motion of the standard fluid rest frames with respect to that of the radiation field (which is, so far, remaining uniform in its own frame). These Doppler corrections can be calculated analytically and the results were presented in the Appendix of [7]. Solely on the basis of this consideration, one finds that f_E is given by $(8/9)u^2(1 + 4u^2/3)^{-1}$. As the bubble grows to dimensions comparable with λ , there is progressive coupling between the radiation and the standard fluid on the relevant length-scales and this interaction tends in the direction of making the radiation more isotropic as seen from the standard fluid. This effect is approximated by multiplying the Doppler term in (5) by a correction factor (in the large brackets) which has the effect of producing the right behaviour in the optically thin and optically thick limits and giving a physically plausible join between them.

The appropriate value of λ is not known accurately but, on the basis of elementary considerations, we have taken $\lambda \approx 10^4$ fm. Tests made in order to investigate the sensitivity of the numerical code to the values adopted for the various parameters will be discussed in Section V.

For the source moments s_0 and s_1 we use the expressions

$$s_0 = \frac{1}{\lambda}(\epsilon - w_0) + (s_0)_{SC}, \quad (6)$$

$$s_1 = -\frac{w_1}{\lambda}, \quad (7)$$

where $(s_0)_{SC}$ is a term expressing the contribution due to scatterings and ϵ is the energy density for radiation in thermal equilibrium with the standard fluid. Assuming that it roughly follows a black-body law, ϵ can be written as

$$\epsilon = g_R \left(\frac{\pi^2}{30} \right) T_F^4, \quad (8)$$

with g_R being the number of degrees of freedom of the radiation fluid and T_F the temperature of the standard fluid.

Obtaining a suitable expression for $(s_0)_{SC}$ is less straightforward. While detailed derivations have been made for simpler applications [13–14], the lack of

precise knowledge about the interaction processes in the present case, has led us express $(s_0)_{sC}$ by the simple absorption and emission term

$$(s_0)_{sC} = \frac{\alpha_2}{\lambda}(\epsilon - w_0), \quad (9)$$

where α_2 is an adjustable coefficient ranging between zero and one. Fortunately, the results of the numerical calculations turn out not to depend sensitively on the value chosen; a discussion of this will be given in Section V.

Equations (1)–(3), describing the processes of transfer between the standard fluid and the radiation fluid, need to be solved together with the hydrodynamic equations

$$u_{,t} = -a \left[\frac{\Gamma}{b} \left(\frac{p_{,\mu} + bs_1}{e + p} \right) + 4\pi GR \left(p + \frac{1}{3}w_0 + w_2 \right) + \frac{GM}{R^2} \right], \quad (10)$$

$$\frac{(\rho R^2)_{,t}}{\rho R^2} = -a \left(\frac{u_{,\mu} - 4\pi GbRw_1}{R_{,\mu}} \right), \quad (11)$$

$$e_{,t} = w\rho_{,t} - as_0, \quad (12)$$

$$\frac{(aw)_{,\mu}}{aw} = -\frac{w\rho_{,\mu} - e_{,\mu} + bs_1}{\rho w}, \quad (13)$$

$$M_{,\mu} = 4\pi R^2 R_{,\mu} \left(e + w_0 + \frac{u}{\Gamma} w_1 \right), \quad (14)$$

$$\Gamma = \left(1 + u^2 - \frac{2GM}{R} \right)^{1/2} = \frac{1}{b} R_{,\mu}, \quad (15)$$

$$b = \frac{1}{4\pi R^2 \rho}. \quad (16)$$

where ρ is the *relative compression factor* (which plays the same role as played by the rest-mass density in a non-relativistic fluid), Γ is the general relativistic analogue of the Lorentz factor, and w is the specific enthalpy ($w = (e + p)/\rho$). The generalized mass function M can also be calculated using the alternative equation

$$M_{,t} = -4\pi R^2 R_{,t} \left(p + \frac{1}{3}w_0 + \frac{\Gamma}{u} w_1 + w_2 \right). \quad (17)$$

Equations of state are required for both phases of the strongly interacting matter. The hadronic medium is taken to consist of massless, pointlike pions for which

$$e_h = g_h \left(\frac{\pi^2}{30} \right) T_h^4 \quad p_h = \frac{1}{3} e_h, \quad (18)$$

while the quark phase is described by the M.I.T. *Bag Model* equation of state [15]

$$e_q = g_q \left(\frac{\pi^2}{30} \right) T_q^4 + B \quad p_q = g_q \left(\frac{\pi^2}{90} \right) T_q^4 - B, \quad (19)$$

where B is the ‘‘Bag’’ constant. We take $g_q = 37$, $g_h = 3$ and these values need to be incremented by the relevant number of additional degrees of freedom g_R when any of the radiative particles are completely coupled to the strongly interacting matter.

For treating the phase interface, we again use a characteristic scheme (as in [7]). The characteristic form of (1), (2), (10) and (12) is

$$du \pm \frac{\Gamma}{\rho w c_s} dp + a \left\{ \frac{\Gamma}{\rho w} (s_1 \pm c_s s_0) + 4\pi GR \left[p + \left(\frac{1}{3} + f_E \right) w_0 \mp c_s w_1 \right] + \frac{GM}{R^2} \pm \frac{2\Gamma u c_s}{R} \right\} dt = 0, \quad (20)$$

which are to be solved along the forward and backward characteristics of the standard fluid $d\mu = \pm (a/b)c_s dt$ (here $c_s = (\partial p/\partial e)^{1/2}$ is the local sound speed in the standard fluid), and

$$\begin{aligned} dw_1 \pm \left(\frac{1}{3} + f_E \right)^{1/2} dw_0 + \left[\left(\frac{4}{3} + f_E \right) w_0 \pm \frac{2(c_s^2 - 1 - K)(1/3 + f_E)^{1/2}}{c_s^2 - 1/3 - f_E} w_1 \right] \frac{1}{\Gamma} du \\ + \left[\frac{2(f_E - 2/3 - K)}{\rho w (c_s^2 - 1/3 - f_E)} \right] w_1 dp + a \left\{ \left(\frac{2u}{R} - \frac{4\pi GR w_1}{\Gamma} \right) \times \right. \\ \times \left[\frac{2[(1/3 + f_E)(c_s^2 - 1) - K c_s^2]}{c_s^2 - 1/3 - f_E} w_1 \pm \left(\frac{4}{3} + f_E \right) \left(\frac{1}{3} + f_E \right)^{1/2} w_0 \right] \\ + \left[4\pi R \left(p + w_0 \left(\frac{1}{3} + f_E \right) \right) + \frac{M}{R^2} \right] \times \\ \times \left[\left(\frac{4}{3} + f_E \right) w_0 \pm \frac{2(c_s^2 - 1 - K)(1/3 + f_E)^{1/2}}{c_s^2 - 1/3 - f_E} w_1 \right] \frac{G}{\Gamma} - \frac{Ku(1 + 4u^2/3)}{\lambda(1 + R/\lambda)} w_1 \\ - \frac{1}{R} \left\{ 3f_E \left[\pm \left(\frac{1}{3} + f_E \right)^{1/2} u - \Gamma \right] w_0 - 2 \left[\pm \left(\frac{1}{3} + f_E \right)^{1/2} \Gamma - u \right] w_1 \right\} \\ + \left[\frac{2c_s^2}{\rho w (c_s^2 - 1/3 - f_E)} \left(f_E - \frac{2}{3} - K \right) w_1 \mp \left(\frac{1}{3} + f_E \right)^{1/2} \right] s_0 \\ + \left. \left[\pm \frac{2}{\rho w (c_s^2 - 1/3 - f_E)} \left(f_E - \frac{2}{3} - K \right) \left(\frac{1}{3} + f_E \right)^{1/2} w_1 - 1 \right] s_1 \right\} dt = 0, \end{aligned} \quad (21)$$

which are to be solved along the forward and backward characteristics of the radiation fluid $d\mu = \pm (a/b)(1/3 + f_E)^{1/2} dt$, and where for compactness we have defined

$$K = f_E \frac{\Gamma w_0}{u(1 + 4u^2/3)w_1}. \quad (22)$$

Supplementary equations calculating ρ , R and M are solved along the flow-lines of the standard fluid (i.e. advective directions $d\mu = 0$) and are

$$d\rho - \frac{1}{c_s^2 w} dp - \frac{as_0}{w} dt = 0, \quad (23)$$

$$dR = au dt, \quad (24)$$

$$dM = -4\pi R^2 au \left[p + \left(\frac{1}{3} + f_E \right) w_0 + \frac{\Gamma}{u} w_1 \right] dt. \quad (25)$$

The configuration of characteristic curves adjacent to the interface is shown in Figure 1 for evolution of the system from time level t to a subsequent time level $t + \Delta t$. The dashed lines represent the forward and backward characteristics for the radiation fluid \mathbf{r} , the full narrow lines are the equivalent characteristics for the standard fluids \mathbf{f} , the vertical dotted line is a flow-line of the standard fluid in the quark phase and the heavy line is the worldline of the interface.

Figure 1. The configuration of characteristic curves near the phase interface drawn in the Lagrangian coordinate frame.

Note that the difference between the characteristic directions results from the difference between the sound speeds in the radiation fluid ($(1/3 + f_E)^{1/2}$) and in the standard fluid (c_s). If the latter were not relativistic, this difference would be large but in the present case $c_s \rightarrow 1/\sqrt{3}$ and the difference between the sound speeds is frequently very small. This leads to some considerable complications in the numerical solution of the equations which we will discuss in Section IV.

To complete the solution at the interface, it is also necessary to introduce junction conditions across it and those for the energy and momentum of the standard fluid can be obtained using the Gauss–Codazzi formalism [16, 17]. Taking

the surface tension σ to be independent of temperature, these junction conditions are

$$[(e + p)ab]^\pm = 0, \quad (26)$$

$$[eb^2\dot{\mu}_s^2 + pa^2]^\pm = -\frac{\sigma f^2}{2} \left\{ \frac{1}{ab} \frac{d}{dt} \left(\frac{b^2\dot{\mu}_s}{f} \right) + \frac{f_{,\mu}}{ab} + \frac{2}{fR} (b\dot{\mu}_s u + a\Gamma) \right\}^\pm, \quad (27)$$

where $[A]^\pm = A^+ - A^-$, $\{A\}^\pm = A^+ + A^-$, μ_s is the interface location, $\dot{\mu}_s = d\mu_s/dt$, $f = (a^2 - b^2\dot{\mu}_s^2)^{1/2}$ and the superscripts $^\pm$ indicate quantities immediately ahead of and behind the interface [5].

Up to the time of the complete coupling, it is reasonable to neglect any interaction of the radiation fluid with the matter in the phase interface and so the energy and momentum junction conditions for the radiation are just continuity conditions:

$$\left[ab\dot{\mu}_s \left(\frac{4}{3} + f_E \right) w_0 - (a^2 + b^2\dot{\mu}_s^2) w_1 \right]^\pm = 0, \quad (28)$$

$$\left[\left\{ a^2 \left(\frac{1}{3} + f_E \right) + b^2\dot{\mu}_s^2 \right\} w_0 - 2ab\dot{\mu}_s w_1 \right]^\pm = 0. \quad (29)$$

Other supplementary junction conditions follow from continuity across the interface of the metric quantities R , dR/dt , and ds

$$[R]^\pm = 0, \quad (30)$$

$$[au + b\dot{\mu}_s\Gamma]^\pm = 0, \quad (31)$$

$$[a^2 - b^2\dot{\mu}_s^2]^\pm = 0, \quad (32)$$

and from the time evolution of the mass function M

$$\frac{d}{dt}[M]^\pm = 4\pi R_s^2 \left[b\Gamma\dot{\mu}_s \left\{ (e + w_0 + \frac{u}{\Gamma}w_1) \right\} - au \left\{ p + \left(\frac{1}{3} + f_E \right) w_0 + \frac{\Gamma}{u}w_1 \right\} \right]^\pm. \quad (33)$$

At the time of bubble nucleation, conditions are essentially Newtonian so that

$$[M]^\pm = 4\pi R_s^2 \sigma. \quad (34)$$

One further equation is needed in order to complete the solution at the interface and this is an expression for the rate at which the quark matter passes across it. A suitable expression is obtained by setting the hydrodynamical flux F_H into the hadron region equal to the net thermal flux F_T into it

$$F_H = \frac{aw\dot{\mu}_s}{4\pi R_s^2(a^2 - b^2\dot{\mu}_s^2)} = \left(\frac{\alpha_1}{4}\right) g_h \left(\frac{\pi^2}{30}\right) (T_q^4 - T_h^4) = F_T \quad (35)$$

where α_1 is an accommodation coefficient ($0 \leq \alpha_1 \leq 1$).

This completes the set of equations. In the next Section we will present the details of the computational scheme and discuss the techniques and the strategies used.

III. Numerical Computations of Bubble Growth

In order to solve the equations of the previous section, we have constructed a computer code following the lines of the one developed previously for calculations of the initial stages of bubble growth (see [7] for a full description). As before, this employs a composite numerical strategy in which a standard Lagrangian finite-difference method is used to solve the hydrodynamical equations in the bulk of each phase, while the system of characteristic equations and junction conditions is solved for the grid zones immediately ahead of and behind the phase interface (which is tracked continuously through the grid). The radiation quantities w_0 and w_2 are taken as “mid-zone” quantities while the radiation flux w_1 is taken as a zone boundary quantity and calculated at the half time level (as for the velocity u – see [7] for details).

The equations presented in Section II are general in nature and can be applied to a variety of situations. Normally, there would be no problem in doing this but some particular difficulties have arisen when applying them to the present case of bubble growth at the cosmological Q–H phase transition. Here, direct use of the radiation equations in the form given above leads to rapidly-growing instabilities which destroy the solution. After a series of experiments it was found that the difficulty originates in the very small deviation of w_0 and w_1 away from their initial values during the early part of the bubble growth, and in the fact that the characteristic sound speed in the radiation fluid $(1/3 + f_E)^{1/2}$ becomes very close to the sound speed in the standard fluid c_s when the radiation is nearly

isotropic in the rest frame of the standard fluid (*i.e.* when $f_E \rightarrow 0$). These features lead to production of cancellation errors in the solution of Eqs. (1) and (2) and near divergences in the characteristic form of the equations (21) (the expression $(c_s^2 - 1/3 - f_E)$ appears in the denominator of several terms). Note that the near equality of the sound speeds only arises when the standard fluid is, itself, relativistic (with $c_s \sim 1/\sqrt{3}$). Also, it is a peculiarity of the present situation that, initially, the radiation is nearly isotropic in the rest frame of the standard fluid not because the medium is optically thick on the scale of the bubble but, rather, because of the assumed isotropy of the universe.

For overcoming the cancellation errors, we have introduced new radiation variables defined as the difference between the energy density, the flux and the shear of the radiation fluid and some reference values (indicated below by the superscript *) with the aim of performing an analytic cancellation of large terms in the equations leaving behind smaller “difference” terms. It turns out to be convenient to take these reference values to be those which would be measured if the only effect were that resulting from the motion of the fluid relative to a uniform radiation field having an energy density equal to that at the time of nucleation of the bubble, $(w_0)_N$. (These are the pure Doppler values mentioned earlier and calculated in the Appendix of [7].) Using a tilde to denote the new variables, we have

$$\tilde{w}_0 = w_0 - (w_0)^* = w_0 - \left(1 + \frac{4}{3}u^2\right)(w_0)_N, \quad (36)$$

$$\tilde{w}_1 = w_1 - (w_1)^* = w_1 + \frac{4}{3}u\Gamma(w_0)_N, \quad (37)$$

$$\tilde{w}_2 = w_2 - (w_2)^* = w_2 - \frac{8}{9}u^2(w_0)_N, \quad (38)$$

and equations (1) and (2) can then be rewritten as

$$\begin{aligned}
& (\tilde{w}_0)_{,t} + a\tilde{w}_0 \left[\frac{1}{R^2} \left(\frac{4}{3} + f_E \right) (uR^2)_{,R} - \frac{3uf_E}{R} \right] + \frac{\Gamma}{aR^2} (\tilde{w}_1 a^2 R^2)_{,R} \\
& \quad + a \frac{4}{3R} (w_0)_N \left[f_E \left(\frac{3}{4} + u^2 \right) - \frac{2}{3} u^2 \right] \left[\frac{1}{R} (uR^2)_{,R} - 3u \right] - as_0 \\
& - \frac{4}{3} a (w_0)_N G \left[4\pi u R \left(2p - e - \frac{w_0}{3} + 2w_2 - \frac{u}{\Gamma} w_1 \right) - \frac{M}{R} \left(2u_{,R} + \frac{u}{R} \right) \right] \\
& \quad - \frac{4\pi a G R}{\Gamma} \left(\frac{4}{3} w_0 + w_2 \right) w_1 = 0,
\end{aligned} \tag{39}$$

$$\begin{aligned}
& (\tilde{w}_1)_{,t} + 2\tilde{w}_1 \frac{a}{R} (uR)_{,R} + a\Gamma \left(\frac{\tilde{w}_0}{3} + \tilde{w}_2 \right)_{,R} + \Gamma \left(\frac{4}{3} \tilde{w}_0 + \tilde{w}_2 \right) a_{,R} + \frac{3a\Gamma\tilde{w}_2}{R} \\
& \quad - as_1 + \frac{4}{3} a (w_0)_N \Gamma G \left[4\pi R \left(p + \frac{w_0}{3} + w_2 - \frac{u}{\Gamma} w_1 \right) + \frac{M}{a^2 R^2} (a^2 R)_{,R} \right] \\
& \quad - \frac{8\pi a G R w_1^2}{\Gamma} = 0,
\end{aligned} \tag{40}$$

where the partial derivatives with respect to μ have been replaced by the equivalent derivatives with respect to R (*i.e.* $\partial/\partial R = (4\pi R^2 \rho/\Gamma) \partial/\partial \mu$). Equations (39) and (40) are the new radiation hydrodynamical equations for the bulk of each phase; once the “tilde” variables have been computed, the values of w_0, w_1, w_2 can be calculated from (36)–(38). Note that in (39), (40) the radiation variables which are multiplied by G are not transformed according to (36)–(38). This has been done to keep the expressions in a simpler form and because the contribution of these terms is small under the present circumstances.

Using the new variables, the radiation characteristic equations become

$$d\tilde{w}_1 \pm \left(\frac{1}{3} + f_E \right)^{1/2} d\tilde{w}_0 + \text{BU} du + \text{BP} dp + \text{BT} dt = 0, \tag{41}$$

where

$$\begin{aligned}
\text{BU} = & \frac{a}{\Gamma} \left\{ \left(\frac{4}{3} + f_E \right) \tilde{w}_0 + \frac{8}{3} (w_0)_N \left(\frac{GM}{R} - \frac{u^2 R}{3(\lambda + R)} \right) \right. \\
& \left. \pm 2 \left(\frac{1}{3} + f_E \right)^{1/2} \left\{ \frac{2\Gamma}{u} \left[\frac{\tilde{w}_0}{(1 + 4u^2/3)} - (w_0)_N \frac{R}{\lambda} \left(1 + \frac{4}{3} u^2 \right) \right] + \frac{4\tilde{w}_1}{3f_E} \right\} \right\},
\end{aligned} \tag{42}$$

$$\text{BP} = \frac{2\Gamma}{\rho w} \left[\frac{\tilde{w}_0}{u(1+4u^2/3)} + \frac{2\tilde{w}_1}{3\Gamma f_E} \left(1 - \frac{3}{2} f_E \right) - (w_0)_N \frac{R}{u\lambda} \left(1 + \frac{4}{3} u^2 \right) \right], \quad (43)$$

$$\begin{aligned} \text{BT} &= \left\{ (\text{BU}) \left\{ 4\pi GR \left[p + \left(\frac{1}{3} + f_E \right) w_0 \right] + \frac{GM}{R^2} + \frac{\Gamma}{\rho w} s_1 \right\} \right. \\ &\quad \left. + \frac{2ac_s^2}{\rho w} (\text{BP}) \left[s_0 + \rho w \left(\frac{2u}{R} - \frac{4\pi GR w_1}{\Gamma} \right) \right] \right\} \\ &+ a \left\{ \tilde{w}_0 \left[\Gamma f_E \frac{(3\lambda + 2R)}{R(\lambda + R)} - \frac{s_1}{\rho w} \left(\frac{4}{3} + f_E \right) \pm \left(\frac{1}{3} + f_E \right)^{1/2} \frac{u}{R} \left(\frac{8}{3} - f_E \right) \right] \right. \\ &\quad \left. + 2\tilde{w}_1 \left[\frac{u}{R} - \frac{4\pi GR w_1}{\Gamma} \pm \left(\frac{1}{3} + f_E \right)^{1/2} \left(\frac{\Gamma}{R} - \frac{s_1}{\rho w} \right) \right] \right. \\ &\quad \left. - \frac{8\Gamma u^2}{9(\lambda + R)} \left[\frac{(4\lambda + 3R)}{(\lambda + R)} \mp \left(\frac{1}{3} + f_E \right)^{1/2} \frac{u}{\Gamma} \right] (w_0)_N \right. \\ &\quad \left. + \frac{4}{3} (w_0)_N \left\{ 4\pi G\Gamma R \left[\left(p + \frac{w_0}{3} + \frac{u}{\Gamma} w_1 + w_2 \right) \right. \right. \right. \\ &\quad \left. \left. \mp \frac{u}{\Gamma} \left(\frac{1}{3} + f_E \right)^{1/2} \left(2p - e - \frac{w_0}{3} - \frac{u}{\Gamma} w_1 + 2w_2 \right) \right] \right. \right. \\ &\quad \left. \left. + \frac{\Gamma GM}{R^2} \left(1 \pm \left(\frac{1}{3} + f_E \right)^{1/2} \frac{u}{\Gamma} \right) \pm \left(\frac{1}{3} + f_E \right)^{1/2} s_0 \right\} \right. \\ &\quad \left. - s_1 \left[1 + \frac{(w_0)_N}{\rho w} \left(\frac{8GM}{3R} - \frac{8u^2 R}{9(\lambda + R)} \right) \right] \right. \\ &\quad \left. \mp \left(\frac{1}{3} + f_E \right)^{1/2} \frac{4\pi GR w_0 w_1}{\Gamma} \left(\frac{4}{3} + f_E \right) \right\} \\ &= (\text{BU}) \left\{ 4\pi GR \left[p + \left(\frac{1}{3} + f_E \right) w_0 \right] + \frac{GM}{R^2} + \frac{\Gamma}{\rho w} s_1 \right\} \\ &\quad + \frac{2ac_s^2}{a\rho w} (\text{BP}) \left[s_0 + \rho w \left(\frac{2u}{R} - \frac{4\pi GR w_1}{\Gamma} \right) \right] + a\overline{\text{BT}}. \end{aligned} \quad (44)$$

The new form of the radiation junction conditions (28) and (29) is

$$\left[ab\dot{\mu}_s \left(\frac{4}{3} + f_E \right) \tilde{w}_0 - (a^2 + b^2\dot{\mu}_s^2)\tilde{w}_1 + (w_0)_N \left\{ ab\dot{\mu}_s \left(1 + \frac{4}{3}u^2 \right) \left(\frac{4}{3} + f_E \right) + \frac{4}{3}u\Gamma(a^2 + b^2\dot{\mu}_s^2) \right\} \right]^\pm = 0, \quad (45)$$

$$\left[\left\{ a^2 \left(\frac{1}{3} + f_E \right) + b^2\dot{\mu}_s^2 \right\} \tilde{w}_0 - 2ab\dot{\mu}_s \tilde{w}_1 + (w_0)_N \left\{ \left(1 + \frac{4}{3}u^2 \right) \left[a^2 \left(\frac{1}{3} + f_E \right) + b^2\dot{\mu}_s^2 \right] + \frac{8}{3}abu\Gamma\dot{\mu}_s \right\} \right]^\pm = 0. \quad (46)$$

Note that the characteristic equation no longer has terms with $(c_s^2 - 1/3 - f_E)$ in the denominator but it *does* have terms containing the ratio \tilde{w}_1/f_E and these still give rise to numerical instabilities. However, this can be countered by further rewriting the equations in a form in which \tilde{w}_1/f_E only appears as the coefficient of expressions which are small when $f_E \rightarrow 0$. The central point in our strategy consists in isolating the group of terms which appears on the left-hand-side of the fluid characteristic equations (20) (and hence tends to zero when $f_E \rightarrow 0$ and the fluid and radiation characteristics coincide). Details of the manipulation involved are given in the Appendix. This group of terms can then be conveniently handled using the differences between parameter values at the feet of the fluid and radiation characteristics. The revised form of the radiation characteristic equations (which is the one actually implemented in the code) is

$$\begin{aligned} d\tilde{w}_1 \pm \left(\frac{1}{3} + f_E \right)^{1/2} d\tilde{w}_0 + BUdu - \frac{2\tilde{w}_1}{(e+p)} dp + BTdt \\ + \frac{c_s}{\Gamma} \left\{ \frac{2\Gamma}{u} \left[\frac{\tilde{w}_0}{1 + 4u^2/3} - (w_0)_N \frac{R}{\lambda} \left(1 + \frac{4}{3}u^2 \right) \right] + \frac{4\tilde{w}_1}{3f_E} \right\} \times \\ \times \left\{ du \pm \frac{\Gamma}{\rho w c_s} dp + a \left\{ \frac{\Gamma}{\rho w} (s_1 \pm c_s s_0) \right. \right. \\ \left. \left. + 4\pi GR \left[p + \left(\frac{1}{3} + f_E \right) w_0 \mp c_s w_1 \right] + \frac{GM}{R^2} \pm \frac{2\Gamma u c_s}{R} \right\} dt \right\} = 0, \end{aligned} \quad (47)$$

where

$$\begin{aligned} \text{BU} = & \frac{a}{\Gamma} \left\{ \left[\left(\frac{4}{3} + f_E \right) \tilde{w}_0 + \frac{8}{3} (w_0)_N \left(\frac{GM}{R} - \frac{u^2 R}{3(\lambda + R)} \right) \right] \right. \\ & \left. \pm \left(\frac{(1/3 + f_E)^{1/2}}{c_s} - 1 \right) \frac{c_s}{\Gamma} \left\{ \frac{2\Gamma}{u} \left[\frac{\tilde{w}_0}{1 + 4u^2/3} - (w_0)_N \frac{R}{\lambda} \left(1 + \frac{4}{3} u^2 \right) \right] + \frac{4\tilde{w}_1}{3f_E} \right\} \right\}, \end{aligned} \quad (48)$$

$$\begin{aligned} \text{BT} = & (\text{BU}) \left\{ G \left\{ 4\pi R \left[p + \left(\frac{1}{3} + f_E \right) w_0 \right] + \frac{M}{R^2} \right\} + \frac{\Gamma}{\rho w} s_1 \right\} \\ & + \frac{2a}{\rho w} c_s^2 \left[s_0 + \rho w \left(\frac{2u}{R} - \frac{4\pi G R w_1}{\Gamma} \right) \right] \left(\frac{4}{3} \Gamma u (w_0)_N - \tilde{w}_1 \right) + a \overline{\text{BT}}, \end{aligned} \quad (49)$$

where $\overline{\text{BT}}$ is the same as in (44). Note that the last two lines of (47) are the terms on the left-hand-side of the standard fluid characteristic equations (20).

IV. Initial conditions

Making use of the experience gained in the earlier work [7], the setting of initial conditions has been quite straightforward. We started with a single super-cooled hadronic bubble nucleated in mechanical and thermal equilibrium with its surroundings at a temperature T_N slightly below the critical temperature for the transition T_C . The equilibrium is an unstable one and any perturbation (continuing expansion of the universe, for example) will cause it to start growing. However, this growth is extremely slow and, in practice, it is not easy to follow with our code as numerical noise rapidly dominates. Our strategy then was to introduce a small artificial perturbation, decreasing the fluid temperature inside the bubble by a small amount below its equilibrium value, and analytically tracing the effect of this on related quantities (including the velocity field of the standard fluid). This successfully produced a suitable data set for starting the time evolution in a smooth and consistent way (see [7]).

Since, at this stage, the radius of the bubble is small compared with λ , the radiation fluid is not significantly affected by the thermal perturbation and remains uniform and isotropic in its own frame. The initial conditions for w_0, w_1, w_2 (measured in the rest frames of the standard fluid) are then those calculated from the Doppler formulae discussed earlier.

V. Tests and results

As usual in numerical computations, the construction of the computer code was followed by a series of tests to eliminate errors and verify that the strategies used were satisfactory. One important test consisted in turning off the source functions and checking that the computed values of the radiation variables agreed with the analytical Doppler expressions. This revealed the problems discussed earlier. When these had been satisfactorily solved, the source functions were then turned on again and complete runs of the code were carried out. As the radius of the bubble increased (leading to increased coupling between the radiation and the standard fluid on relevant length scales) care was required as increasingly steep gradients of w_0 appeared in the vicinity of the interface prior to complete coupling. Since structure on a scale smaller than the grid spacing can obviously not be resolved, it is necessary to be ready to switch on complete coupling in the equations at the appropriate moment. Some experimentation was required in order to do this in the best way. When this had been done, further tests were carried out in order to examine the sensitivity of the results to changes in the physical parameters and assumptions. In the following, we will first present results for a set of “canonical” parameter values and then discuss the effect of varying some of these.

In Figs. 2 – 5, we show results from a run with $T_C = 150$ MeV, $T_N/T_C = 0.98$, $\sigma_0 = 1$, $\alpha_1 = \alpha_2 = 1$ and $\lambda = 10^4$ fm. Here $\sigma_0 = \sigma/T_C^3$ is a parameter commonly used to measure the relative strength of the surface tension. The value which we are taking for this is larger than currently preferred ones but we give results for this case to allow direct comparison with those of [7]. Figs. 2 and 3 show the behaviour of the velocity and energy density of the standard fluid, at various times during the bubble growth, while Figs. 4 and 5 show the corresponding behaviour of the radiation energy density and flux. All of these figures should be viewed together and it is useful, also, to make comparison with Figs. 2 and 4 of [7] which are for the equivalent calculation without inclusion of the radiation particles. (Note that for convenience in drawing these figures, the values of the variables at the centre of the bubble have been plotted at $\log_{10}R(\text{fm}) = 0$ rather than at $R = 0$.)

During the first part of the bubble expansion ($R_s \lesssim 10^2$ fm), the standard fluid variables behave in an identical way to that seen previously in the calculation with no radiative transfer: the velocity of the interface progressively increases and a compression wave is pushed out into the surrounding quark medium. The

velocity profile in the quark phase is approximately solenoidal ($u \propto 1/R^2$). The radiation variables at this stage have profiles which are almost exactly the Doppler ones produced by the motion of the fluid relative to an essentially uniform radiation field. In the previous calculations, where radiative transfer was not included, the standard fluid variables tended towards a similarity solution which was effectively attained for $R_s \gtrsim 10^3$ fm. In the present calculation, the coupling together of the radiation and the standard fluid (which can be clearly seen in Fig. 4) starts to be effective before the former similarity solution is fully reached, causing first a distortion of the velocity profile and subsequently a decrease in the peak velocity. (If a smaller value is used for σ_0 , both bubble nucleation and the attainment of the similarity solution occur at smaller values of R_s .) As the coupling becomes more complete on the relevant length scales (when $R_s \sim 10^4$ fm), the peak of the radiation flux profile becomes very narrow (the main part of the flux is concentrated exactly at the interface) and when it is no longer possible to resolve this on the grid we switch to total coupling. This involves setting to zero the radiation flux w_1 , the Eddington factor f_E and the source functions s_0 and s_1 and augmenting the number of degrees of freedom for the standard fluid at the interface to include also those of the coupled radiation. The behaviour of the radiation at the interface is then included together with that of the standard fluid. Following the total coupling, the variables tend rapidly to a new similarity solution characterized by smaller velocities (the front now has to push a medium having larger inertia) and a smaller temperature jump across the interface.

Figures 2–3. Velocity of the standard fluid u and energy density e . Different curves are for different times during the bubble growth; the dashed lines represent the values at the initial time. Here $\alpha_2 = 1$ and $\lambda = 10^4$ fm.

Figures 4–5. Radiation fluid energy density w_0 and energy flux w_1 . Here $\alpha_2 = 1$ and $\lambda = 10^4$ fm.

Next, we turn to a discussion of the effect on the results of varying the values taken for some of the physical parameters. Bearing in mind the discussion already given in [7], we will concentrate here just on the mean-free-path for the radiation particles λ (whose value has an uncertainty of about an order of magnitude), and on the coefficient α_2 appearing in the expression for the source moment s_0 (Eq. (9)).

Figures 6–7. Radiation energy density w_0 and standard fluid velocity u just ahead of the phase interface and just behind it (higher and lower curves respectively). The curves are the result of calculations with different values of λ ; R_s is the bubble radius and $\alpha_2 = 1$. The curves are plotted so that the hadronic region is on the left of the discontinuity tracing the phase interface.

The effect produced by varying λ is illustrated in Figures 6 and 7, which show the behaviour during the bubble expansion of the values of w_0 and u measured just ahead of the interface and just behind it. The different values of λ used (which are represented with the different styles of line) are 5×10^3 fm, 10^4 fm and 10^5 fm, proceeding from left to right. As one would expect, use of a larger value of λ has the effect of causing the coupling to occur when the bubble has reached a larger value of R_s .

Figures 8–9. Radiation energy density w_0 and standard fluid velocity u just ahead of the phase interface and just behind it. The curves are the result of calculations with different values of the non-conservative scattering coefficient α_2 . Here $\lambda = 10^4$ fm.

Figures 8 and 9 show the effect of varying the coefficient for the non-conservative scatterings (α_2). The different values of α_2 used are 0, 0.5 and 1; the larger values give an increased rate of energy transfer and make the total coupling occur earlier.

These tests show that although the results can indeed be influenced by different choices of the parameters, there is no serious qualitative change. We have also checked on the sensitivity of the code to the form chosen for the Eddington factor f_E . (The background to our choice for this was discussed in Section II.) In our investigation, we have modified the form given in Eq. (5) by replacing the monotonic correction term $\lambda/(\lambda + R)$ with a more sophisticated expression having a maximum whose position and the amplitude could be suitably tuned in different combinations. Paying attention to producing a smooth join between the optically-thin and optically-thick limits, we have found that reasonable variations in this joining function lead to only minor differences in the results, confirming previous experience [13, 14].

VI. Conclusion

In this paper, we have presented a study of the hydrodynamics of the cosmological quark-hadron transition in the presence of long-range energy and momentum transfer by electromagnetically and weakly interacting particles. The relativistic radiative transfer problem for the generalized radiation fluid has been treated using the PSTF tensor formalism. A system of Lagrangian hydrodynamical equations has been presented which has then been solved numerically by means of a computer code which uses a standard Lagrangian finite difference scheme for flow within the bulk of each phase together with a characteristic method for the vicinity of the phase interface across which relativistic junction conditions are solved. The results show the progressive coupling together of the strongly-interacting matter and the radiation fluid as the bubble expands. When the complete coupling occurs, there is no dramatic effect on the bubble which simply decreases its expansion velocity and the eventually approaches a similarity solution.

Work is now in progress in order to extend this treatment to the final stages of the transition during which the evaporation of disconnected quark droplets occurs. At these stages, which are of great interest in connection with possible consequences of the transition, long-range energy and momentum transport certainly play an important role.

Acknowledgements

We gratefully acknowledge helpful discussions with Ornella Pantano, Roberto Turolla and Luca Zampieri. Financial support for this research has been provided by the Italian Ministero dell'Università e della Ricerca Scientifica e Tecnologica.

References

- [1] F. Karsch and E. Laermann, Rep. Prog. Phys., *in press* (1994).
- [2] J. Ignatius, K. Kajantie, H. Kurki-Suonio and M. Laine, Phys. Rev. D **49**, 3854 (1994).
- [3] J. Ignatius, K. Kajantie, H. Kurki-Suonio and M. Laine, Phys. Rev. D **50**, 3738 (1994).
- [4] B. Cheng and A. Olinto, Phys. Rev. D **50**, 2421 (1994).
- [5] O. Pantano, Phys. Lett. B **224**, 195 (1989).
- [6] J.C. Miller and O. Pantano, Phys. Rev. D **40**, 1789 (1989).
- [7] J.C. Miller and O. Pantano, Phys. Rev. D **42**, 3334 (1990).
- [8] L. Rezzolla and J.C. Miller, Class. Quantum Grav. **11**, 1815 (1994).
- [9] H. Kurki-Suonio H, Phys. Rev. D **37**, 2104 (1988).
- [10] E. Witten, Phys. Rev. D **30**, 272 (1984).
- [11] K.S. Thorne, M.N.R.A.S. **194**, 439 (1981).
- [12] K.S. Thorne, R.A. Flammang and A. Zytchow, M.N.R.A.S. **194**, 475 (1981).
- [13] L. Nobili, R. Turolla and L. Zampieri, Ap. J. **383**, 250 (1991).
- [14] L. Nobili, R. Turolla and L. Zampieri, Ap. J. **404**, 686 (1993).
- [15] A. Chodos, R.L. Jaffe, K. Johnson, C.B. Thorn and V.F. Weisskopf, Phys. Rev. D **9**, 3471 (1974).
- [16] W. Israel, Il Nuovo Cimento **44**, 1 (1966).
- [17] K. Maeda, General Relativity and Gravitation **18**, 931 (1986).

Appendix

In this Appendix we outline the calculations by means of which the radiation characteristic equations (41)–(44) are rewritten in the new form (47)–(49). The aim is to make the ratio \tilde{w}_1/f_E the coefficient of a quantity which is small when $f_E \rightarrow 0$ and in order to do this we have first isolated the terms in (41) where this ratio appears:

$$\begin{aligned}
& \frac{4\tilde{w}_1}{3\Gamma f_E} \left\{ \pm \left(\frac{1}{3} + f_E \right)^{1/2} du + \frac{\Gamma}{\rho w} \left(1 - \frac{3}{2} f_E \right) dp \right. \\
& \pm a \left(\frac{1}{3} + f_E \right)^{1/2} \left\{ 4\pi GR \left[p + \left(\frac{1}{3} + f_E \right) w_0 \right] + \frac{GM}{R^2} + \frac{\Gamma}{\rho w} s_1 \right\} dt \\
& \left. + ac_s^2 \frac{\Gamma}{\rho w} \left(1 - \frac{3}{2} f_E \right) \left[s_0 + \rho w \left(\frac{2u}{R} - \frac{4\pi GR w_1}{\Gamma} \right) \right] dt \right\}.
\end{aligned} \tag{A1}$$

This can be rearranged to give

$$\begin{aligned}
& \pm \frac{4\tilde{w}_1}{3\Gamma f_E} \left\{ \left[\left(\frac{1}{3} + f_E \right)^{1/2} - c_s \right] du \mp \frac{3\Gamma}{2\rho w} f_E dp \right. \\
& + a \left[\left(\frac{1}{3} + f_E \right)^{1/2} - c_s \right] \left\{ 4\pi GR \left[p + \left(\frac{1}{3} + f_E \right) w_0 \right] + \frac{GM}{R^2} + \frac{\Gamma}{\rho w} s_1 \right\} dt \\
& \left. \mp \frac{3\Gamma}{2\rho w} f_E ac_s^2 \left[s_0 + \rho w \left(\frac{2u}{R} - \frac{4\pi GR w_1}{\Gamma} \right) \right] dt \right\} \\
& \pm \frac{4\tilde{w}_1}{3\Gamma f_E} c_s \left\{ du \pm \frac{\Gamma}{\rho w c_s} dp + a \left\{ \frac{\Gamma}{\rho w} (s_1 \pm c_s s_0) \right. \right. \\
& \left. \left. + 4\pi GR \left[p + \left(\frac{1}{3} + f_E \right) w_0 \mp c_s w_1 \right] + \frac{GM}{R^2} \pm \frac{2\Gamma u c_s}{R} \right\} dt \right\}.
\end{aligned} \tag{A2}$$

Replacing (A1) by (A2) then leads to the expressions (47)–(49) which are the new characteristic equations for the radiation fluid. Note that the manipulation has produced two major effects: firstly it has introduced terms which are intrinsically small when $f_E \rightarrow 0$ (such as the difference between the sound speeds or f_E itself), and secondly it has brought together a set of terms which coincides with those on the left-hand-side of the standard fluid characteristic equation but are now evaluated along the characteristic directions of the radiation fluid. The sum of these terms becomes very small when f_E is small so that the two sets of characteristics nearly coincide.

Hydrodynamics of the cosmological quark-hadron transition in the presence of long-range energy and momentum transfer

John C. Miller^{1,2,3} & Luciano Rezzolla¹

¹Scuola Internazionale Superiore di Studi Avanzati, Trieste, Italy.

²Department of Physics, University of Oxford, England.

³Osservatorio Astronomico di Trieste, Trieste, Italy.

Abstract

Two previous papers in this series have presented a study of the growth of hadronic bubbles during the cosmological Quark–Hadron transition, treating the material within each phase as a single perfect fluid. Here, we extend the analysis to include the effects of long-range energy and momentum transfer by weakly and electromagnetically interacting particles. After a short review of the formalism adopted, we discuss the numerical strategies used in the computer code which has been constructed in order to solve this system of equations. Results for the growth of single hadronic bubbles are also presented.

PACS Nos.: 47.55.Dz, 47.75.+f, 95.30.Jx, 98.80.Cq

SISSA Ref. 161/94/A-EP (Oct 94)

I. Introduction

At about $10 \mu\text{s}$ after the big bang it is thought that strongly interacting matter underwent a transition from a plasma of free quarks and gluons to one in which the quarks were confined within hadrons (predominantly pions). Current lattice-gauge calculations [1] favour the view that this change may well have been a continuous one, but the possibility of it being a first order phase transition is by no means ruled out and considerable interest continues to be focussed on the astrophysical consequences which might have arisen if it was, indeed, first order (see, for example [2–4]).

The work described here (which is part of an ongoing research programme [5–8]) is within the scenario of a first-order transition starting with the nucleation of hadronic bubbles in a slightly supercooled quark-gluon plasma. The bubbles then proceed to grow (with the quark-gluon plasma being progressively transformed into a hadronic one) until eventually they coalesce and give rise to disconnected quark regions which then shrink and probably disappear completely (possibly leaving behind a significant baryon-number inhomogeneity) [9] but might instead reach a stable configuration composed of *strange quark matter* [10].

In the earlier papers of the series, attention has been focussed on studying the hydrodynamics of the growth of single hadronic bubbles during the initial stages of the transition where it makes sense to consider the material in each phase as a perfect fluid composed only of the strongly interacting matter. While the transition involves only these particles in a direct way, an important role is also played by other particles present, which can interact with them through the electromagnetic and weak interactions: primarily photons, electrons, muons and their antiparticles (electromagnetic and weak interactions) and neutrinos and antineutrinos (weak interaction only). All of these have mean free paths long compared with that of the strongly interacting matter and can provide a mechanism for long-range transport of energy and momentum through the strongly interacting fluid. Since the leptons concerned are essentially massless, both they and the photons can be treated as components of a generalized “radiation fluid” and the problem is then one of relativistic radiative transfer.

During bubble growth, the effect of this transport becomes significant when the radius R_s of the bubble surface becomes roughly comparable with the mean free path λ of the particles concerned ($\sim 10^4$ fermi for the electromagnetic interaction and ~ 1 cm for the weak interaction). When $R_s \ll \lambda$, the bubble is

essentially transparent to the radiation, which can then be ignored, while when $R_s \gg \lambda$ the coupling is essentially complete on relevant length-scales so that the radiation and strongly interacting matter move together as a single fluid. Clearly, the process of coupling can, in principle, occur twice during the bubble growth, but because the behaviour is similar in each case, we will discuss here only the one occurring between the strongly interacting and electromagnetically interacting particles. Identical considerations apply also for the coupling with the neutrinos, the only difference, apart from the scale, being the different number of degrees of freedom into which the energy liberated by the transition is channeled.

This paper is concerned with adding the effects of radiative transfer to our earlier scheme of calculation for following bubble growth [7], thus extending its range of validity. Subsequently, we aim to apply a similar scheme to the last stage of the transition (shrinking away of the disconnected quark regions) which is likely to give rise to the most interesting consequences from an astrophysical point of view. The formalism used for handling the radiative transfer has been the subject of an earlier paper [8] and only a brief outline of this will be presented again here.

The plan of the paper is as follows. In Section II we give a short review of the equations and then Section III describes the outline of our computational scheme which uses a combined characteristic and Lagrangian finite-difference approach. Some particular problems arise in the computational implementation and we explain how these have been overcome by means of introducing new variables for the radiation fluid. Section IV concerns the setting up of initial conditions, Section V describes tests carried out and results obtained and Section VI is the conclusion. Throughout, we use a system of units in which $c = \hbar = k_B = 1$ and a space-like signature $(-, +, +, +)$. Greek indices are taken to run from 0 to 3 and Latin indices from 1 to 3; covariant derivatives are denoted with a semi-colon and partial derivatives with a comma.

II. Relativistic Hydrodynamical Equations

This section contains a short review of the equations used in the rest of the paper. A full discussion of these has already been presented in [8] to which the reader is referred for further details and references.

The transfer of energy and momentum is considered as taking place between a *standard fluid*, composed of the strongly interacting particles and any other

particles effectively moving together with them, and a *radiation fluid* consisting of those particles responsible for the long-range transfer of energy and momentum. We treat the transfer using the PSTF (Projected Symmetric Trace Free) tensor formalism of Thorne [11], [12] in which the relativistic radiative transfer equation is rewritten in terms of an infinite hierarchy of differential equations involving PSTF moments which is then truncated by introducing suitable closure relations. For spherical symmetry, the tensor formalism becomes effectively a scalar one. We made the truncation at second order and obtained

$$(w_0)_{,t} + \frac{a}{b}(w_1)_{,\mu} + \frac{4}{3}\left(\frac{b_{,t}}{b} + \frac{2R_{,t}}{R}\right)w_0 + \frac{2a}{b}\left(\frac{a_{,\mu}}{a} + \frac{R_{,\mu}}{R}\right)w_1 + \left(\frac{b_{,t}}{b} - \frac{R_{,t}}{R}\right)w_2 = as_0, \quad (1)$$

$$(w_1)_{,t} + \frac{a}{b}\left(\frac{1}{3}w_0 + w_2\right)_{,\mu} + \frac{4a_{,\mu}}{3b}w_0 + 2\left(\frac{b_{,t}}{b} + \frac{R_{,t}}{R}\right)w_1 + \frac{a}{b}\left(\frac{a_{,\mu}}{a} + \frac{3R_{,\mu}}{R}\right)w_2 = as_1, \quad (2)$$

$$w_2 = f_E w_0, \quad (3)$$

where w_0 is the energy density of the radiation, w_1 is the radiation flux and w_2 is the anisotropy scalar of the radiation (all measured in the local rest frame of the standard fluid); s_0 and s_1 are energy and momentum source functions and a and b are metric coefficients of the spherically symmetric line element

$$ds^2 = -a^2 dt^2 + b^2 d\mu^2 + R^2(d\theta^2 + \sin^2\theta d\varphi^2), \quad (4)$$

where μ is a comoving radial coordinate and R is the associated Eulerean coordinate (the Schwarzschild circumference coordinate).

The quantity f_E appearing in the closure relation (3) is a *variable Eddington factor* which can take values ranging from 0, for complete isotropy (which could be caused by the medium being extremely optically thick), to $2/3$ for complete anisotropy (which might arise when the medium is very optically thin). The expression used for it has to be arrived at on the basis of physical considerations and for our case we have used

$$f_E \equiv \frac{8u^2/9}{(1 + 4u^2/3)} \left(\frac{\lambda}{\lambda + R} \right), \quad (5)$$

where λ is the effective mean-free-path of the radiation particles. In our picture, the bubble is first nucleated within a uniform and isotropic quark medium and the radiation field (which interacts with the quark medium on suitably large scales and is in thermal equilibrium with it) initially shares these properties (*i.e.* w_0 is

constant everywhere and w_1 and w_2 are zero). The radius of the newly-formed bubble is small compared with λ and the medium is essentially transparent to the radiation on this scale. As the bubble starts to expand, the radiation quantities deviate from their values at the time of nucleation primarily as a result of the Doppler effect arising from the motion of the standard fluid rest frames with respect to that of the radiation field (which is, so far, remaining uniform in its own frame). These Doppler corrections can be calculated analytically and the results were presented in the Appendix of [7]. Solely on the basis of this consideration, one finds that f_E is given by $(8/9)u^2(1 + 4u^2/3)^{-1}$. As the bubble grows to dimensions comparable with λ , there is progressive coupling between the radiation and the standard fluid on the relevant length-scales and this interaction tends in the direction of making the radiation more isotropic as seen from the standard fluid. This effect is approximated by multiplying the Doppler term in (5) by a correction factor (in the large brackets) which has the effect of producing the right behaviour in the optically thin and optically thick limits and giving a physically plausible join between them.

The appropriate value of λ is not known accurately but, on the basis of elementary considerations, we have taken $\lambda \approx 10^4$ fm. Tests made in order to investigate the sensitivity of the numerical code to the values adopted for the various parameters will be discussed in Section V.

For the source moments s_0 and s_1 we use the expressions

$$s_0 = \frac{1}{\lambda}(\epsilon - w_0) + (s_0)_{SC}, \quad (6)$$

$$s_1 = -\frac{w_1}{\lambda}, \quad (7)$$

where $(s_0)_{SC}$ is a term expressing the contribution due to scatterings and ϵ is the energy density for radiation in thermal equilibrium with the standard fluid. Assuming that it roughly follows a black-body law, ϵ can be written as

$$\epsilon = g_R \left(\frac{\pi^2}{30} \right) T_F^4, \quad (8)$$

with g_R being the number of degrees of freedom of the radiation fluid and T_F the temperature of the standard fluid.

Obtaining a suitable expression for $(s_0)_{SC}$ is less straightforward. While detailed derivations have been made for simpler applications [13–14], the lack of

precise knowledge about the interaction processes in the present case, has led us express $(s_0)_{s_C}$ by the simple absorption and emission term

$$(s_0)_{s_C} = \frac{\alpha_2}{\lambda}(\epsilon - w_0), \quad (9)$$

where α_2 is an adjustable coefficient ranging between zero and one. Fortunately, the results of the numerical calculations turn out not to depend sensitively on the value chosen; a discussion of this will be given in Section V.

Equations (1)–(3), describing the processes of transfer between the standard fluid and the radiation fluid, need to be solved together with the hydrodynamic equations

$$u_{,t} = -a \left[\frac{\Gamma}{b} \left(\frac{p_{,\mu} + bs_1}{e + p} \right) + 4\pi GR \left(p + \frac{1}{3}w_0 + w_2 \right) + \frac{GM}{R^2} \right], \quad (10)$$

$$\frac{(\rho R^2)_{,t}}{\rho R^2} = -a \left(\frac{u_{,\mu} - 4\pi GbRw_1}{R_{,\mu}} \right), \quad (11)$$

$$e_{,t} = w\rho_{,t} - as_0, \quad (12)$$

$$\frac{(aw)_{,\mu}}{aw} = -\frac{w\rho_{,\mu} - e_{,\mu} + bs_1}{\rho w}, \quad (13)$$

$$M_{,\mu} = 4\pi R^2 R_{,\mu} \left(e + w_0 + \frac{u}{\Gamma} w_1 \right), \quad (14)$$

$$\Gamma = \left(1 + u^2 - \frac{2GM}{R} \right)^{1/2} = \frac{1}{b} R_{,\mu}, \quad (15)$$

$$b = \frac{1}{4\pi R^2 \rho}. \quad (16)$$

where ρ is the *relative compression factor* (which plays the same role as played by the rest-mass density in a non-relativistic fluid), Γ is the general relativistic analogue of the Lorentz factor, and w is the specific enthalpy ($w = (e + p)/\rho$). The generalized mass function M can also be calculated using the alternative equation

$$M_{,t} = -4\pi R^2 R_{,t} \left(p + \frac{1}{3}w_0 + \frac{\Gamma}{u} w_1 + w_2 \right). \quad (17)$$

Equations of state are required for both phases of the strongly interacting matter. The hadronic medium is taken to consist of massless, pointlike pions for which

$$e_h = g_h \left(\frac{\pi^2}{30} \right) T_h^4 \quad p_h = \frac{1}{3} e_h, \quad (18)$$

while the quark phase is described by the M.I.T. *Bag Model* equation of state [15]

$$e_q = g_q \left(\frac{\pi^2}{30} \right) T_q^4 + B \quad p_q = g_q \left(\frac{\pi^2}{90} \right) T_q^4 - B, \quad (19)$$

where B is the ‘‘Bag’’ constant. We take $g_q = 37$, $g_h = 3$ and these values need to be incremented by the relevant number of additional degrees of freedom g_R when any of the radiative particles are completely coupled to the strongly interacting matter.

For treating the phase interface, we again use a characteristic scheme (as in [7]). The characteristic form of (1), (2), (10) and (12) is

$$\begin{aligned} du \pm \frac{\Gamma}{\rho w c_s} dp + a \left\{ \frac{\Gamma}{\rho w} (s_1 \pm c_s s_0) \right. \\ \left. + 4\pi G R \left[p + \left(\frac{1}{3} + f_E \right) w_0 \mp c_s w_1 \right] + \frac{GM}{R^2} \pm \frac{2\Gamma u c_s}{R} \right\} dt = 0, \end{aligned} \quad (20)$$

which are to be solved along the forward and backward characteristics of the standard fluid $d\mu = \pm (a/b)c_s dt$ (here $c_s = (\partial p/\partial e)^{1/2}$ is the local sound speed in the standard fluid), and

$$\begin{aligned} dw_1 \pm \left(\frac{1}{3} + f_E \right)^{1/2} dw_0 + \left[\left(\frac{4}{3} + f_E \right) w_0 \pm \frac{2(c_s^2 - 1 - K)(1/3 + f_E)^{1/2}}{c_s^2 - 1/3 - f_E} w_1 \right] \frac{1}{\Gamma} du \\ + \left[\frac{2(f_E - 2/3 - K)}{\rho w (c_s^2 - 1/3 - f_E)} \right] w_1 dp + a \left\{ \left(\frac{2u}{R} - \frac{4\pi G R w_1}{\Gamma} \right) \times \right. \\ \left. \times \left[\frac{2[(1/3 + f_E)(c_s^2 - 1) - K c_s^2]}{c_s^2 - 1/3 - f_E} w_1 \pm \left(\frac{4}{3} + f_E \right) \left(\frac{1}{3} + f_E \right)^{1/2} w_0 \right] \right. \\ \left. + \left[4\pi R \left(p + w_0 \left(\frac{1}{3} + f_E \right) \right) + \frac{M}{R^2} \right] \times \right. \\ \left. \times \left[\left(\frac{4}{3} + f_E \right) w_0 \pm \frac{2(c_s^2 - 1 - K)(1/3 + f_E)^{1/2}}{c_s^2 - 1/3 - f_E} w_1 \right] \frac{G}{\Gamma} - \frac{K u (1 + 4u^2/3)}{\lambda(1 + R/\lambda)} w_1 \right. \\ \left. - \frac{1}{R} \left\{ 3f_E \left[\pm \left(\frac{1}{3} + f_E \right)^{1/2} u - \Gamma \right] w_0 - 2 \left[\pm \left(\frac{1}{3} + f_E \right)^{1/2} \Gamma - u \right] w_1 \right\} \right. \\ \left. + \left[\frac{2c_s^2}{\rho w (c_s^2 - 1/3 - f_E)} \left(f_E - \frac{2}{3} - K \right) w_1 \mp \left(\frac{1}{3} + f_E \right)^{1/2} \right] s_0 \right. \\ \left. + \left[\pm \frac{2}{\rho w (c_s^2 - 1/3 - f_E)} \left(f_E - \frac{2}{3} - K \right) \left(\frac{1}{3} + f_E \right)^{1/2} w_1 - 1 \right] s_1 \right\} dt = 0, \end{aligned} \quad (21)$$

which are to be solved along the forward and backward characteristics of the radiation fluid $d\mu = \pm (a/b)(1/3 + f_E)^{1/2} dt$, and where for compactness we have defined

$$K = f_E \frac{\Gamma w_0}{u(1 + 4u^2/3)w_1}. \quad (22)$$

Supplementary equations calculating ρ , R and M are solved along the flow-lines of the standard fluid (i.e. advective directions $d\mu = 0$) and are

$$d\rho - \frac{1}{c_s^2 w} dp - \frac{as_0}{w} dt = 0, \quad (23)$$

$$dR = au dt, \quad (24)$$

$$dM = -4\pi R^2 au \left[p + \left(\frac{1}{3} + f_E \right) w_0 + \frac{\Gamma}{u} w_1 \right] dt. \quad (25)$$

The configuration of characteristic curves adjacent to the interface is shown in Figure 1 for evolution of the system from time level t to a subsequent time level $t + \Delta t$. The dashed lines represent the forward and backward characteristics for the radiation fluid r , the full narrow lines are the equivalent characteristics for the standard fluids f , the vertical dotted line is a flow-line of the standard fluid in the quark phase and the heavy line is the worldline of the interface.

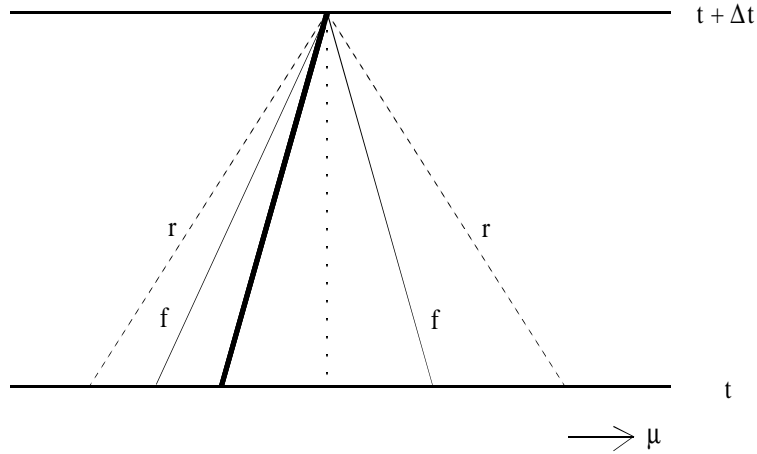


Figure 1. The configuration of characteristic curves near the phase interface drawn in the Lagrangian coordinate frame.

Note that the difference between the characteristic directions results from the difference between the sound speeds in the radiation fluid $((1/3 + f_E)^{1/2})$ and in the standard fluid (c_s) . If the latter were not relativistic, this difference would

be large but in the present case $c_s \rightarrow 1/\sqrt{3}$ and the difference between the sound speeds is frequently very small. This leads to some considerable complications in the numerical solution of the equations which we will discuss in Section IV.

To complete the solution at the interface, it is also necessary to introduce junction conditions across it and those for the energy and momentum of the standard fluid can be obtained using the Gauss–Codazzi formalism [16, 17]. Taking the surface tension σ to be independent of temperature, these junction conditions are

$$[(e + p)ab]^\pm = 0, \quad (26)$$

$$[eb^2\dot{\mu}_s^2 + pa^2]^\pm = -\frac{\sigma f^2}{2} \left\{ \frac{1}{ab} \frac{d}{dt} \left(\frac{b^2 \dot{\mu}_s}{f} \right) + \frac{f_{,\mu}}{ab} + \frac{2}{fR} (b\dot{\mu}_s u + a\Gamma) \right\}^\pm, \quad (27)$$

where $[A]^\pm = A^+ - A^-$, $\{A\}^\pm = A^+ + A^-$, μ_s is the interface location, $\dot{\mu}_s = d\mu_s/dt$, $f = (a^2 - b^2\dot{\mu}_s^2)^{1/2}$ and the superscripts \pm indicate quantities immediately ahead of and behind the interface [5].

Up to the time of the complete coupling, it is reasonable to neglect any interaction of the radiation fluid with the matter in the phase interface and so the energy and momentum junction conditions for the radiation are just continuity conditions:

$$\left[ab\dot{\mu}_s \left(\frac{4}{3} + f_E \right) w_0 - (a^2 + b^2\dot{\mu}_s^2) w_1 \right]^\pm = 0, \quad (28)$$

$$\left[\left\{ a^2 \left(\frac{1}{3} + f_E \right) + b^2\dot{\mu}_s^2 \right\} w_0 - 2ab\dot{\mu}_s w_1 \right]^\pm = 0. \quad (29)$$

Other supplementary junction conditions follow from continuity across the interface of the metric quantities R , dR/dt , and ds

$$[R]^\pm = 0, \quad (30)$$

$$[au + b\dot{\mu}_s \Gamma]^\pm = 0, \quad (31)$$

$$[a^2 - b^2\dot{\mu}_s^2]^\pm = 0, \quad (32)$$

and from the time evolution of the mass function M

$$\frac{d}{dt}[M]^\pm = 4\pi R_s^2 \left[b\Gamma\dot{\mu}_s \left\{ (e + w_0 + \frac{u}{\Gamma}w_1) \right\} - au \left\{ p + \left(\frac{1}{3} + f_E \right) w_0 + \frac{\Gamma}{u}w_1 \right\} \right]^\pm. \quad (33)$$

At the time of bubble nucleation, conditions are essentially Newtonian so that

$$[M]^\pm = 4\pi R_s^2 \sigma. \quad (34)$$

One further equation is needed in order to complete the solution at the interface and this is an expression for the rate at which the quark matter passes across it. A suitable expression is obtained by setting the hydrodynamical flux F_H into the hadron region equal to the net thermal flux F_T into it

$$F_H = \frac{aw\dot{\mu}_s}{4\pi R_s^2(a^2 - b^2\dot{\mu}_s^2)} = \left(\frac{\alpha_1}{4}\right) g_h \left(\frac{\pi^2}{30}\right) (T_q^4 - T_h^4) = F_T \quad (35)$$

where α_1 is an accommodation coefficient ($0 \leq \alpha_1 \leq 1$).

This completes the set of equations. In the next Section we will present the details of the computational scheme and discuss the techniques and the strategies used.

III. Numerical Computations of Bubble Growth

In order to solve the equations of the previous section, we have constructed a computer code following the lines of the one developed previously for calculations of the initial stages of bubble growth (see [7] for a full description). As before, this employs a composite numerical strategy in which a standard Lagrangian finite-difference method is used to solve the hydrodynamical equations in the bulk of each phase, while the system of characteristic equations and junction conditions is solved for the grid zones immediately ahead of and behind the phase interface (which is tracked continuously through the grid). The radiation quantities w_0 and w_2 are taken as “mid-zone” quantities while the radiation flux w_1 is taken as a zone boundary quantity and calculated at the half time level (as for the velocity u – see [7] for details).

The equations presented in Section II are general in nature and can be applied to a variety of situations. Normally, there would be no problem in doing this but some particular difficulties have arisen when applying them to the present case of bubble growth at the cosmological Q–H phase transition. Here, direct use of the radiation equations in the form given above leads to rapidly-growing instabilities which destroy the solution. After a series of experiments it was found that the

difficulty originates in the very small deviation of w_0 and w_1 away from their initial values during the early part of the bubble growth, and in the fact that the characteristic sound speed in the radiation fluid $(1/3 + f_E)^{1/2}$ becomes very close to the sound speed in the standard fluid c_s when the radiation is nearly isotropic in the rest frame of the standard fluid (*i.e.* when $f_E \rightarrow 0$). These features lead to production of cancellation errors in the solution of Eqs. (1) and (2) and near divergences in the characteristic form of the equations (21) (the expression $(c_s^2 - 1/3 - f_E)$ appears in the denominator of several terms). Note that the near equality of the sound speeds only arises when the standard fluid is, itself, relativistic (with $c_s \sim 1/\sqrt{3}$). Also, it is a peculiarity of the present situation that, initially, the radiation is nearly isotropic in the rest frame of the standard fluid not because the medium is optically thick on the scale of the bubble but, rather, because of the assumed isotropy of the universe.

For overcoming the cancellation errors, we have introduced new radiation variables defined as the difference between the energy density, the flux and the shear of the radiation fluid and some reference values (indicated below by the superscript *) with the aim of performing an analytic cancellation of large terms in the equations leaving behind smaller “difference” terms. It turns out to be convenient to take these reference values to be those which would be measured if the only effect were that resulting from the motion of the fluid relative to a uniform radiation field having an energy density equal to that at the time of nucleation of the bubble, $(w_0)_N$. (These are the pure Doppler values mentioned earlier and calculated in the Appendix of [7].) Using a tilde to denote the new variables, we have

$$\tilde{w}_0 = w_0 - (w_0)^* = w_0 - \left(1 + \frac{4}{3}u^2\right)(w_0)_N, \quad (36)$$

$$\tilde{w}_1 = w_1 - (w_1)^* = w_1 + \frac{4}{3}u\Gamma(w_0)_N, \quad (37)$$

$$\tilde{w}_2 = w_2 - (w_2)^* = w_2 - \frac{8}{9}u^2(w_0)_N, \quad (38)$$

and equations (1) and (2) can then be rewritten as

$$\begin{aligned}
& (\tilde{w}_0)_{,t} + a\tilde{w}_0 \left[\frac{1}{R^2} \left(\frac{4}{3} + f_E \right) (uR^2)_{,R} - \frac{3uf_E}{R} \right] + \frac{\Gamma}{aR^2} (\tilde{w}_1 a^2 R^2)_{,R} \\
& \quad + a \frac{4}{3R} (w_0)_N \left[f_E \left(\frac{3}{4} + u^2 \right) - \frac{2}{3} u^2 \right] \left[\frac{1}{R} (uR^2)_{,R} - 3u \right] - a s_0 \\
& - \frac{4}{3} a (w_0)_N G \left[4\pi u R \left(2p - e - \frac{w_0}{3} + 2w_2 - \frac{u}{\Gamma} w_1 \right) - \frac{M}{R} \left(2u_{,R} + \frac{u}{R} \right) \right] \\
& \quad - \frac{4\pi a G R}{\Gamma} \left(\frac{4}{3} w_0 + w_2 \right) w_1 = 0,
\end{aligned} \tag{39}$$

$$\begin{aligned}
& (\tilde{w}_1)_{,t} + 2\tilde{w}_1 \frac{a}{R} (uR)_{,R} + a\Gamma \left(\frac{\tilde{w}_0}{3} + \tilde{w}_2 \right)_{,R} + \Gamma \left(\frac{4}{3} \tilde{w}_0 + \tilde{w}_2 \right) a_{,R} + \frac{3a\Gamma \tilde{w}_2}{R} \\
& - a s_1 + \frac{4}{3} a (w_0)_N \Gamma G \left[4\pi R \left(p + \frac{w_0}{3} + w_2 - \frac{u}{\Gamma} w_1 \right) + \frac{M}{a^2 R^2} (a^2 R)_{,R} \right] \\
& \quad - \frac{8\pi a G R w_1^2}{\Gamma} = 0,
\end{aligned} \tag{40}$$

where the partial derivatives with respect to μ have been replaced by the equivalent derivatives with respect to R (*i.e.* $\partial/\partial R = (4\pi R^2 \rho/\Gamma)\partial/\partial\mu$). Equations (39) and (40) are the new radiation hydrodynamical equations for the bulk of each phase; once the “tilde” variables have been computed, the values of w_0, w_1, w_2 can be calculated from (36)–(38). Note that in (39), (40) the radiation variables which are multiplied by G are not transformed according to (36)–(38). This has been done to keep the expressions in a simpler form and because the contribution of these terms is small under the present circumstances.

Using the new variables, the radiation characteristic equations become

$$d\tilde{w}_1 \pm \left(\frac{1}{3} + f_E \right)^{1/2} d\tilde{w}_0 + \text{BU} du + \text{BP} dp + \text{BT} dt = 0, \tag{41}$$

where

$$\begin{aligned}
\text{BU} = & \frac{a}{\Gamma} \left\{ \left(\frac{4}{3} + f_E \right) \tilde{w}_0 + \frac{8}{3} (w_0)_N \left(\frac{GM}{R} - \frac{u^2 R}{3(\lambda + R)} \right) \right. \\
& \left. \pm 2 \left(\frac{1}{3} + f_E \right)^{1/2} \left\{ \frac{2\Gamma}{u} \left[\frac{\tilde{w}_0}{(1 + 4u^2/3)} - (w_0)_N \frac{R}{\lambda} \left(1 + \frac{4}{3} u^2 \right) \right] + \frac{4\tilde{w}_1}{3f_E} \right\} \right\},
\end{aligned} \tag{42}$$

$$\text{BP} = \frac{2\Gamma}{\rho w} \left[\frac{\tilde{w}_0}{u(1 + 4u^2/3)} + \frac{2\tilde{w}_1}{3\Gamma f_E} \left(1 - \frac{3}{2}f_E \right) - (w_0)_N \frac{R}{u\lambda} \left(1 + \frac{4}{3}u^2 \right) \right], \quad (43)$$

$$\begin{aligned} \text{BT} &= \left\{ (\text{BU}) \left\{ 4\pi GR \left[p + \left(\frac{1}{3} + f_E \right) w_0 \right] + \frac{GM}{R^2} + \frac{\Gamma}{\rho w} s_1 \right\} \right. \\ &\quad \left. + \frac{2ac_s^2}{\rho w} (\text{BP}) \left[s_0 + \rho w \left(\frac{2u}{R} - \frac{4\pi GR w_1}{\Gamma} \right) \right] \right. \\ &+ a \left\{ \tilde{w}_0 \left[\Gamma f_E \frac{(3\lambda + 2R)}{R(\lambda + R)} - \frac{s_1}{\rho w} \left(\frac{4}{3} + f_E \right) \pm \left(\frac{1}{3} + f_E \right)^{1/2} \frac{u}{R} \left(\frac{8}{3} - f_E \right) \right] \right. \\ &\quad \left. + 2\tilde{w}_1 \left[\frac{u}{R} - \frac{4\pi GR w_1}{\Gamma} \pm \left(\frac{1}{3} + f_E \right)^{1/2} \left(\frac{\Gamma}{R} - \frac{s_1}{\rho w} \right) \right] \right. \\ &\quad \left. - \frac{8\Gamma u^2}{9(\lambda + R)} \left[\frac{(4\lambda + 3R)}{(\lambda + R)} \mp \left(\frac{1}{3} + f_E \right)^{1/2} \frac{u}{\Gamma} \right] (w_0)_N \right. \\ &\quad \left. + \frac{4}{3} (w_0)_N \left\{ 4\pi G\Gamma R \left[\left(p + \frac{w_0}{3} + \frac{u}{\Gamma} w_1 + w_2 \right) \right. \right. \right. \\ &\quad \left. \left. \mp \frac{u}{\Gamma} \left(\frac{1}{3} + f_E \right)^{1/2} \left(2p - e - \frac{w_0}{3} - \frac{u}{\Gamma} w_1 + 2w_2 \right) \right] \right. \right. \\ &\quad \left. \left. + \frac{\Gamma GM}{R^2} \left(1 \pm \left(\frac{1}{3} + f_E \right)^{1/2} \frac{u}{\Gamma} \right) \pm \left(\frac{1}{3} + f_E \right)^{1/2} s_0 \right\} \right. \\ &\quad \left. - s_1 \left[1 + \frac{(w_0)_N}{\rho w} \left(\frac{8GM}{3R} - \frac{8u^2 R}{9(\lambda + R)} \right) \right] \right. \\ &\quad \left. \mp \left(\frac{1}{3} + f_E \right)^{1/2} \frac{4\pi GR w_0 w_1}{\Gamma} \left(\frac{4}{3} + f_E \right) \right\} \left. \right\} \\ &= (\text{BU}) \left\{ 4\pi GR \left[p + \left(\frac{1}{3} + f_E \right) w_0 \right] + \frac{GM}{R^2} + \frac{\Gamma}{\rho w} s_1 \right\} \\ &\quad + \frac{2ac_s^2}{a\rho w} (\text{BP}) \left[s_0 + \rho w \left(\frac{2u}{R} - \frac{4\pi GR w_1}{\Gamma} \right) \right] + a\overline{\text{BT}}. \end{aligned} \quad (44)$$

The new form of the radiation junction conditions (28) and (29) is

$$\left[ab\dot{\mu}_s \left(\frac{4}{3} + f_E \right) \tilde{w}_0 - (a^2 + b^2 \dot{\mu}_s^2) \tilde{w}_1 + (w_0)_N \left\{ ab\dot{\mu}_s \left(1 + \frac{4}{3} u^2 \right) \left(\frac{4}{3} + f_E \right) + \frac{4}{3} u \Gamma (a^2 + b^2 \dot{\mu}_s^2) \right\} \right]^\pm = 0, \quad (45)$$

$$\left[\left\{ a^2 \left(\frac{1}{3} + f_E \right) + b^2 \dot{\mu}_s^2 \right\} \tilde{w}_0 - 2ab\dot{\mu}_s \tilde{w}_1 + (w_0)_N \left\{ \left(1 + \frac{4}{3} u^2 \right) \left[a^2 \left(\frac{1}{3} + f_E \right) + b^2 \dot{\mu}_s^2 \right] + \frac{8}{3} abu \Gamma \dot{\mu}_s \right\} \right]^\pm = 0. \quad (46)$$

Note that the characteristic equation no longer has terms with $(c_s^2 - 1/3 - f_E)$ in the denominator but it *does* have terms containing the ratio \tilde{w}_1/f_E and these still give rise to numerical instabilities. However, this can be countered by further rewriting the equations in a form in which \tilde{w}_1/f_E only appears as the coefficient of expressions which are small when $f_E \rightarrow 0$. The central point in our strategy consists in isolating the group of terms which appears on the left-hand-side of the fluid characteristic equations (20) (and hence tends to zero when $f_E \rightarrow 0$ and the fluid and radiation characteristics coincide). Details of the manipulation involved are given in the Appendix. This group of terms can then be conveniently handled using the differences between parameter values at the feet of the fluid and radiation characteristics. The revised form of the radiation characteristic equations (which is the one actually implemented in the code) is

$$\begin{aligned} d\tilde{w}_1 \pm \left(\frac{1}{3} + f_E \right)^{1/2} d\tilde{w}_0 + BU du - \frac{2\tilde{w}_1}{(e+p)} dp + BT dt \\ + \frac{c_s}{\Gamma} \left\{ \frac{2\Gamma}{u} \left[\frac{\tilde{w}_0}{1 + 4u^2/3} - (w_0)_N \frac{R}{\lambda} \left(1 + \frac{4}{3} u^2 \right) \right] + \frac{4\tilde{w}_1}{3f_E} \right\} \times \\ \times \left\{ du \pm \frac{\Gamma}{\rho w c_s} dp + a \left\{ \frac{\Gamma}{\rho w} (s_1 \pm c_s s_0) \right. \right. \\ \left. \left. + 4\pi G R \left[p + \left(\frac{1}{3} + f_E \right) w_0 \mp c_s w_1 \right] + \frac{GM}{R^2} \pm \frac{2\Gamma u c_s}{R} \right\} dt \right\} = 0, \end{aligned} \quad (47)$$

where

$$\begin{aligned} \text{BU} = & \frac{a}{\Gamma} \left\{ \left[\left(\frac{4}{3} + f_E \right) \tilde{w}_0 + \frac{8}{3} (w_0)_N \left(\frac{GM}{R} - \frac{u^2 R}{3(\lambda + R)} \right) \right] \right. \\ & \left. \pm \left(\frac{(1/3 + f_E)^{1/2}}{c_s} - 1 \right) \frac{c_s}{\Gamma} \left\{ \frac{2\Gamma}{u} \left[\frac{\tilde{w}_0}{1 + 4u^2/3} - (w_0)_N \frac{R}{\lambda} \left(1 + \frac{4}{3} u^2 \right) \right] + \frac{4\tilde{w}_1}{3f_E} \right\} \right\}, \end{aligned} \quad (48)$$

$$\begin{aligned} \text{BT} = & (\text{BU}) \left\{ G \left\{ 4\pi R \left[p + \left(\frac{1}{3} + f_E \right) w_0 \right] + \frac{M}{R^2} \right\} + \frac{\Gamma}{\rho w} s_1 \right\} \\ & + \frac{2a}{\rho w} c_s^2 \left[s_0 + \rho w \left(\frac{2u}{R} - \frac{4\pi G R w_1}{\Gamma} \right) \right] \left(\frac{4}{3} \Gamma u (w_0)_N - \tilde{w}_1 \right) + a \overline{\text{BT}}, \end{aligned} \quad (49)$$

where $\overline{\text{BT}}$ is the same as in (44). Note that the last two lines of (47) are the terms on the left-hand-side of the standard fluid characteristic equations (20).

IV. Initial conditions

Making use of the experience gained in the earlier work [7], the setting of initial conditions has been quite straightforward. We started with a single supercooled hadronic bubble nucleated in mechanical and thermal equilibrium with its surroundings at a temperature T_N slightly below the critical temperature for the transition T_C . The equilibrium is an unstable one and any perturbation (continuing expansion of the universe, for example) will cause it to start growing. However, this growth is extremely slow and, in practice, it is not easy to follow with our code as numerical noise rapidly dominates. Our strategy then was to introduce a small artificial perturbation, decreasing the fluid temperature inside the bubble by a small amount below its equilibrium value, and analytically tracing the effect of this on related quantities (including the velocity field of the standard fluid). This successfully produced a suitable data set for starting the time evolution in a smooth and consistent way (see [7]).

Since, at this stage, the radius of the bubble is small compared with λ , the radiation fluid is not significantly affected by the thermal perturbation and remains uniform and isotropic in its own frame. The initial conditions for w_0, w_1, w_2 (measured in the rest frames of the standard fluid) are then those calculated from the Doppler formulae discussed earlier.

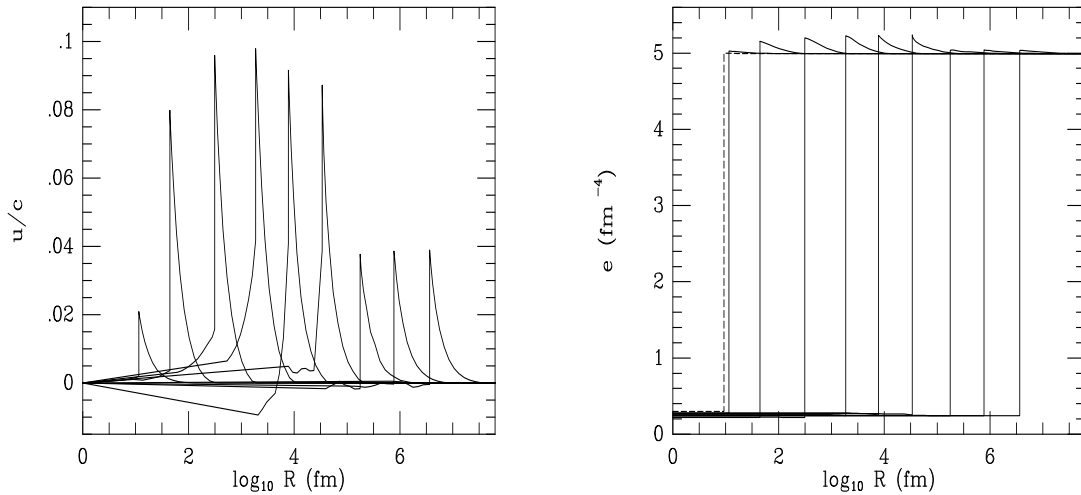
V. Tests and results

As usual in numerical computations, the construction of the computer code was followed by a series of tests to eliminate errors and verify that the strategies used were satisfactory. One important test consisted in turning off the source functions and checking that the computed values of the radiation variables agreed with the analytical Doppler expressions. This revealed the problems discussed earlier. When these had been satisfactorily solved, the source functions were then turned on again and complete runs of the code were carried out. As the radius of the bubble increased (leading to increased coupling between the radiation and the standard fluid on relevant length scales) care was required as increasingly steep gradients of w_0 appeared in the vicinity of the interface prior to complete coupling. Since structure on a scale smaller than the grid spacing can obviously not be resolved, it is necessary to be ready to switch on complete coupling in the equations at the appropriate moment. Some experimentation was required in order to do this in the best way. When this had been done, further tests were carried out in order to examine the sensitivity of the results to changes in the physical parameters and assumptions. In the following, we will first present results for a set of “canonical” parameter values and then discuss the effect of varying some of these.

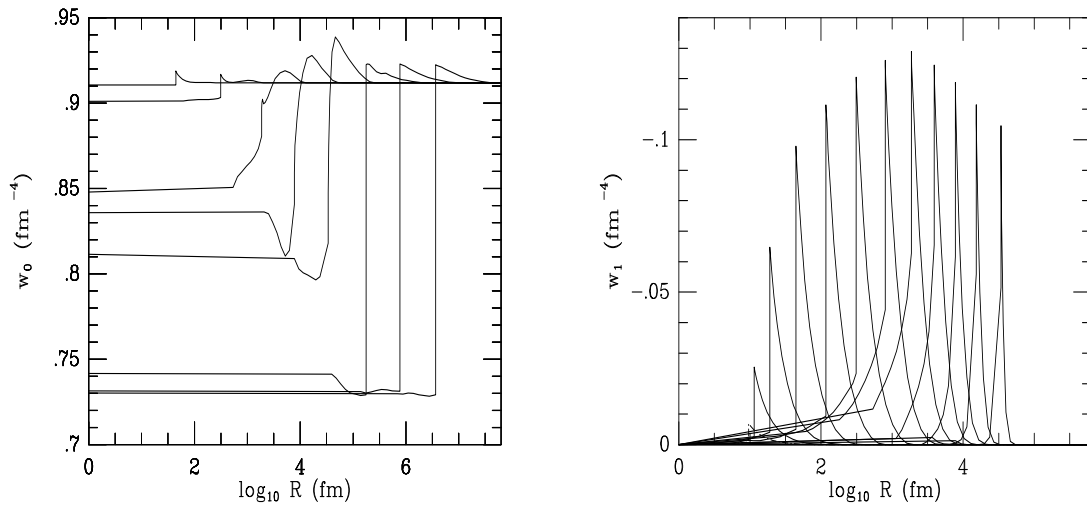
In Figs. 2 – 5, we show results from a run with $T_c = 150$ MeV, $T_N/T_c = 0.98$, $\sigma_0 = 1$, $\alpha_1 = \alpha_2 = 1$ and $\lambda = 10^4$ fm. Here $\sigma_0 = \sigma/T_c^3$ is a parameter commonly used to measure the relative strength of the surface tension. The value which we are taking for this is larger than currently preferred ones but we give results for this case to allow direct comparison with those of [7]. Figs. 2 and 3 show the behaviour of the velocity and energy density of the standard fluid, at various times during the bubble growth, while Figs. 4 and 5 show the corresponding behaviour of the radiation energy density and flux. All of these figures should be viewed together and it is useful, also, to make comparison with Figs. 2 and 4 of [7] which are for the equivalent calculation without inclusion of the radiation particles. (Note that for convenience in drawing these figures, the values of the variables at the centre of the bubble have been plotted at $\log_{10} R(\text{fm}) = 0$ rather than at $R = 0$.)

During the first part of the bubble expansion ($R_s \lesssim 10^2$ fm), the standard fluid variables behave in an identical way to that seen previously in the calculation with no radiative transfer: the velocity of the interface progressively increases and a compression wave is pushed out into the surrounding quark medium. The

velocity profile in the quark phase is approximately solenoidal ($u \propto 1/R^2$). The radiation variables at this stage have profiles which are almost exactly the Doppler ones produced by the motion of the fluid relative to an essentially uniform radiation field. In the previous calculations, where radiative transfer was not included, the standard fluid variables tended towards a similarity solution which was effectively attained for $R_s \gtrsim 10^3$ fm. In the present calculation, the coupling together of the radiation and the standard fluid (which can be clearly seen in Fig. 4) starts to be effective before the former similarity solution is fully reached, causing first a distortion of the velocity profile and subsequently a decrease in the peak velocity. (If a smaller value is used for σ_0 , both bubble nucleation and the attainment of the similarity solution occur at smaller values of R_s .) As the coupling becomes more complete on the relevant length scales (when $R_s \sim 10^4$ fm), the peak of the radiation flux profile becomes very narrow (the main part of the flux is concentrated exactly at the interface) and when it is no longer possible to resolve this on the grid we switch to total coupling. This involves setting to zero the radiation flux w_1 , the Eddington factor f_E and the source functions s_0 and s_1 and augmenting the number of degrees of freedom for the standard fluid at the interface to include also those of the coupled radiation. The behaviour of the radiation at the interface is then included together with that of the standard fluid. Following the total coupling, the variables tend rapidly to a new similarity solution characterized by smaller velocities (the front now has to push a medium having larger inertia) and a smaller temperature jump across the interface.

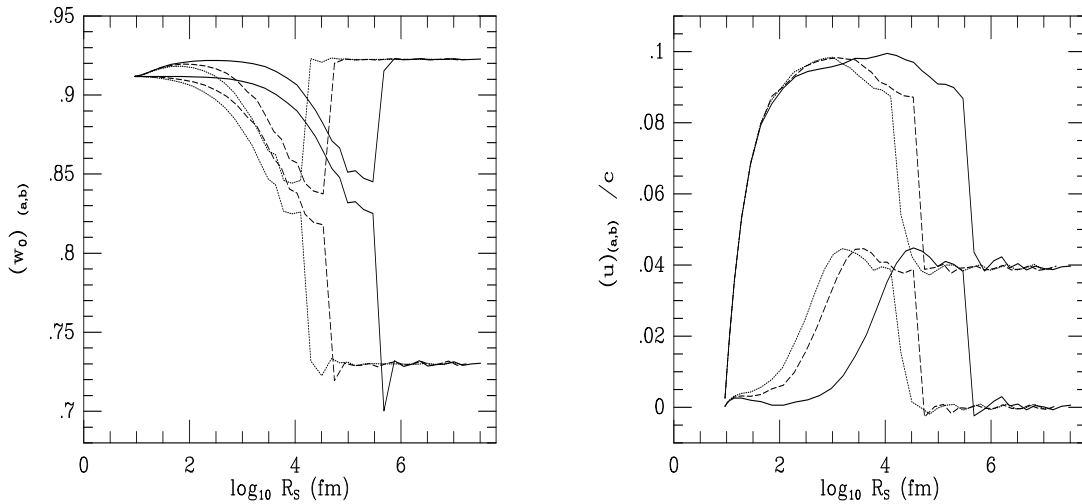


Figures 2–3. Velocity of the standard fluid u and energy density e . Different curves are for different times during the bubble growth; the dashed lines represent the values at the initial time. Here $\alpha_2 = 1$ and $\lambda = 10^4$ fm.



Figures 4-5. Radiation fluid energy density w_0 and energy flux w_1 . Here $\alpha_2 = 1$ and $\lambda = 10^4$ fm.

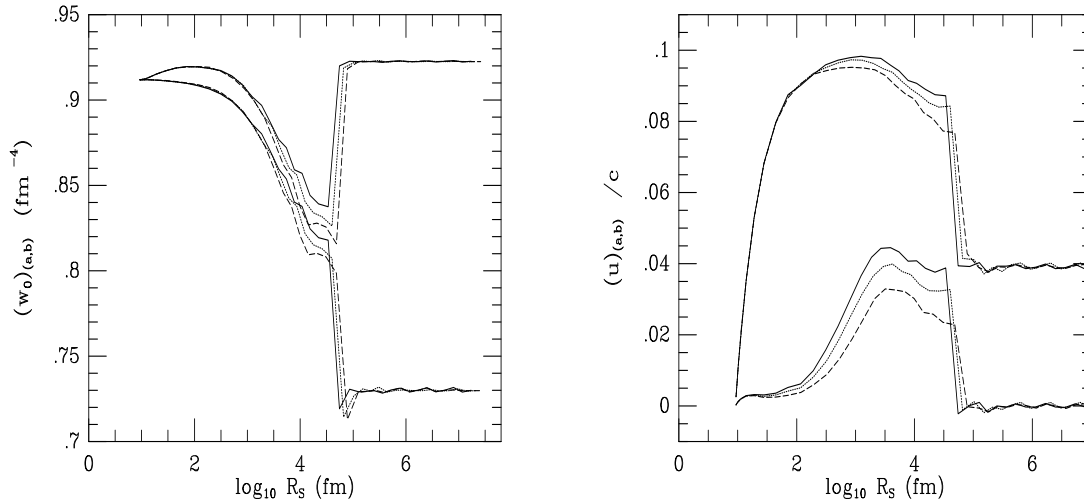
Next, we turn to a discussion of the effect on the results of varying the values taken for some of the physical parameters. Bearing in mind the discussion already given in [7], we will concentrate here just on the mean-free-path for the radiation particles λ (whose value has an uncertainty of about an order of magnitude), and on the coefficient α_2 appearing in the expression for the source moment s_0 (Eq. (9)).



Figures 6-7. Radiation energy density w_0 and standard fluid velocity u just ahead of the phase interface and just behind it (higher and lower curves respectively). The curves are the result of calculations with different values of λ ; R_s is the bubble radius and $\alpha_2 = 1$. The curves are plotted so that the hadronic region is on the left of the discontinuity tracing the phase interface.

The effect produced by varying λ is illustrated in Figures 6 and 7, which show the behaviour during the bubble expansion of the values of w_0 and u measured just

ahead of the interface and just behind it. The different values of λ used (which are represented with the different styles of line) are 5×10^3 fm, 10^4 fm and 10^5 fm, proceeding from left to right. As one would expect, use of a larger value of λ has the effect of causing the coupling to occur when the bubble has reached a larger value of R_s .



Figures 8–9. Radiation energy density w_0 and standard fluid velocity u just ahead of the phase interface and just behind it. The curves are the result of calculations with different values of the non-conservative scattering coefficient α_2 . Here $\lambda = 10^4$ fm.

Figures 8 and 9 show the effect of varying the coefficient for the non-conservative scatterings (α_2). The different values of α_2 used are 0, 0.5 and 1; the larger values give an increased rate of energy transfer and make the total coupling occur earlier.

These tests show that although the results can indeed be influenced by different choices of the parameters, there is no serious qualitative change. We have also checked on the sensitivity of the code to the form chosen for the Eddington factor f_E . (The background to our choice for this was discussed in Section II.) In our investigation, we have modified the form given in Eq. (5) by replacing the monotonic correction term $\lambda/(\lambda + R)$ with a more sophisticated expression having a maximum whose position and the amplitude could be suitably tuned in different combinations. Paying attention to producing a smooth join between the optically-thin and optically-thick limits, we have found that reasonable variations in this joining function lead to only minor differences in the results, confirming previous experience [13, 14].

VI. Conclusion

In this paper, we have presented a study of the hydrodynamics of the cosmological quark-hadron transition in the presence of long-range energy and momentum transfer by electromagnetically and weakly interacting particles. The relativistic radiative transfer problem for the generalized radiation fluid has been treated using the PSTF tensor formalism. A system of Lagrangian hydrodynamical equations has been presented which has then been solved numerically by means of a computer code which uses a standard Lagrangian finite difference scheme for flow within the bulk of each phase together with a characteristic method for the vicinity of the phase interface across which relativistic junction conditions are solved. The results show the progressive coupling together of the strongly-interacting matter and the radiation fluid as the bubble expands. When the complete coupling occurs, there is no dramatic effect on the bubble which simply decreases its expansion velocity and the eventually approaches a similarity solution.

Work is now in progress in order to extend this treatment to the final stages of the transition during which the evaporation of disconnected quark droplets occurs. At these stages, which are of great interest in connection with possible consequences of the transition, long-range energy and momentum transport certainly play an important role.

Acknowledgements

We gratefully acknowledge helpful discussions with Ornella Pantano, Roberto Turolla and Luca Zampieri. Financial support for this research has been provided by the Italian Ministero dell'Università e della Ricerca Scientifica e Tecnologica.

References

- [1] F. Karsch and E. Laermann, Rep. Prog. Phys., *in press* (1994).
- [2] J. Ignatius, K. Kajantie, H. Kurki-Suonio and M. Laine, Phys. Rev. D **49**, 3854 (1994).
- [3] J. Ignatius, K. Kajantie, H. Kurki-Suonio and M. Laine, Phys. Rev. D **50**, 3738 (1994).
- [4] B. Cheng and A. Olinto, Phys. Rev. D **50**, 2421 (1994).
- [5] O. Pantano, Phys. Lett. B **224**, 195 (1989).
- [6] J.C. Miller and O. Pantano, Phys. Rev. D **40**, 1789 (1989).
- [7] J.C. Miller and O. Pantano, Phys. Rev. D **42**, 3334 (1990).
- [8] L. Rezzolla and J.C. Miller, Class. Quantum Grav. **11**, 1815 (1994).
- [9] H. Kurki-Suonio H, Phys. Rev. D **37**, 2104 (1988).
- [10] E. Witten, Phys. Rev. D **30**, 272 (1984).
- [11] K.S. Thorne, M.N.R.A.S. **194**, 439 (1981).
- [12] K.S. Thorne, R.A. Flammang and A. Zytchow, M.N.R.A.S. **194**, 475 (1981).
- [13] L. Nobili, R. Turolla and L. Zampieri, Ap. J. **383**, 250 (1991).
- [14] L. Nobili, R. Turolla and L. Zampieri, Ap. J. **404**, 686 (1993).
- [15] A. Chodos, R.L. Jaffe, K. Johnson, C.B. Thorn and V.F. Weisskopf, Phys. Rev. D **9**, 3471 (1974).
- [16] W. Israel, Il Nuovo Cimento **44**, 1 (1966).
- [17] K. Maeda, General Relativity and Gravitation **18**, 931 (1986).

Appendix

In this Appendix we outline the calculations by means of which the radiation characteristic equations (41)–(44) are rewritten in the new form (47)–(49). The aim is to make the ratio \tilde{w}_1/f_E the coefficient of a quantity which is small when $f_E \rightarrow 0$ and in order to do this we have first isolated the terms in (41) where this ratio appears:

$$\begin{aligned} & \frac{4\tilde{w}_1}{3\Gamma f_E} \left\{ \pm \left(\frac{1}{3} + f_E \right)^{1/2} du + \frac{\Gamma}{\rho w} \left(1 - \frac{3}{2} f_E \right) dp \right. \\ & \pm a \left(\frac{1}{3} + f_E \right)^{1/2} \left\{ 4\pi G R \left[p + \left(\frac{1}{3} + f_E \right) w_0 \right] + \frac{GM}{R^2} + \frac{\Gamma}{\rho w} s_1 \right\} dt \\ & \left. + a c_s^2 \frac{\Gamma}{\rho w} \left(1 - \frac{3}{2} f_E \right) \left[s_0 + \rho w \left(\frac{2u}{R} - \frac{4\pi G R w_1}{\Gamma} \right) \right] dt \right\}. \end{aligned} \tag{A1}$$

This can be rearranged to give

$$\begin{aligned} & \pm \frac{4\tilde{w}_1}{3\Gamma f_E} \left\{ \left[\left(\frac{1}{3} + f_E \right)^{1/2} - c_s \right] du \mp \frac{3\Gamma}{2\rho w} f_E dp \right. \\ & + a \left[\left(\frac{1}{3} + f_E \right)^{1/2} - c_s \right] \left\{ 4\pi G R \left[p + \left(\frac{1}{3} + f_E \right) w_0 \right] + \frac{GM}{R^2} + \frac{\Gamma}{\rho w} s_1 \right\} dt \\ & \mp \frac{3\Gamma}{2\rho w} f_E a c_s^2 \left[s_0 + \rho w \left(\frac{2u}{R} - \frac{4\pi G R w_1}{\Gamma} \right) \right] dt \left. \right\} \\ & \pm \frac{4\tilde{w}_1}{3\Gamma f_E} c_s \left\{ du \pm \frac{\Gamma}{\rho w c_s} dp + a \left\{ \frac{\Gamma}{\rho w} (s_1 \pm c_s s_0) \right. \right. \\ & \left. \left. + 4\pi G R \left[p + \left(\frac{1}{3} + f_E \right) w_0 \mp c_s w_1 \right] + \frac{GM}{R^2} \pm \frac{2\Gamma u c_s}{R} \right\} dt \right\}. \end{aligned} \tag{A2}$$

Replacing (A1) by (A2) then leads to the expressions (47)–(49) which are the new characteristic equations for the radiation fluid. Note that the manipulation has produced two major effects: firstly it has introduced terms which are intrinsically small when $f_E \rightarrow 0$ (such as the difference between the sound speeds or f_E itself), and secondly it has brought together a set of terms which coincides with those on the left-hand-side of the standard fluid characteristic equation but are now evaluated along the characteristic directions of the radiation fluid. The sum of these terms becomes very small when f_E is small so that the two sets of characteristics nearly coincide.